Climate change has altered zooplankton-fuelled carbon export in the North Atlantic

Brun, Philipp Georg; Stamieszkin, Karen ; Visser, Andre W.; Licandro, Priscilla; Payne, Mark; Kiørboe, Thomas

Published in:
Nature Ecology & Evolution

Link to article, DOI:
10.1038/s41559-018-0780-3

Publication date:
2019

Document Version
Peer reviewed version

Climate change has altered zooplankton-fuelled carbon export in the North Atlantic

Philipp Brun[1,2,*], Karen Stamieszkin[3,4], Andre W. Visser[1], Priscilla Licandro[5,6,7], Mark R. Payne[1], and Thomas Kiørboe[1]

[1]Centre for Ocean Life, National Institute of Aquatic Resources, Technical University of Denmark, Kgs. Lyngby, Denmark

[2]Dynamic Macroecology Group, WSL, Zuercherstrasse 111, CH-8903, Birmensdorf, Switzerland

[3]School of Marine Sciences, 360 Aubert Hall, University of Maine, Orono, Maine 04469-5706, USA

[4]Bigelow Laboratory for Ocean Sciences, 60 Bigelow Drive, East Boothbay, Maine USA

[5]Sir Alister Hardy Foundation for Ocean Science, The Laboratory, Citadel Hill, Plymouth PL1 2PB, United Kingdom

[6]Plymouth Marine Laboratory, Prospect Place, The Hoe, Plymouth, PL1 3DH, United Kingdom

[7]Stazione Zoologica Anton Dohrn, Villa Comunale, 80121 Napoli, Italy

*Correspondence to: Philipp Brun (philipp.brun@wsl.ch)

Introductory paragraph

Marine plankton have been conspicuously affected by recent climate change, responding with profound spatial relocations, and shifts in the timing of their seasonal occurrence. These changes directly impact the global carbon cycle by altering the transport of organic material from the surface ocean to depth, with consequences that remain poorly understood. We investigated how distributional and abundance changes of copepods, the dominant group of zooplankton, have affected biogenic carbon cycling. We used trait-based, mechanistic models to estimate the magnitude of carbon transported downward through sinking fecal pellets, daily vertical migration, and seasonal hibernation at depth. From such estimates for over 200,000 community observations in the northern North Atlantic we found carbon flux increases along the northwestern boundary of the study area and decreases in the open northern North Atlantic during the past 55 years. These changes in export were primarily associated with changes in copepod biomass, which were driven by shifting distributions of abundant, large-bodied species. Our findings highlight how recent climate change has fundamentally impacted downward carbon transport by altering copepod community structure, and demonstrate how carbon fluxes through plankton communities can be mechanistically implemented in next-generation biogeochemical models with size-structured representations of zooplankton communities.

Main text

Introduction

The various processes by which organic material is transported from the surface ocean to depth are collectively called the biological pump and remove roughly the same amount of carbon from the atmosphere as humanity has been emitting in recent years[1,2]. Surface-layer copepods contribute to the biological pump through the production of sinking fecal pellets, shed exoskeletons and carcasses, and by conducting vertical migrations[3]. Fecal pellets are compact aggregates of organic material with dimensions proportional to the size of the organism producing them[4,5]. Small fecal pellets produced by small copepods sink more slowly and are thus subject to a greater degree of remineralization, delivering proportionately less carbon to depth. Zooplankton fecal pellets can reach depths of 1000 meters or more, and are commonly found in sediment traps throughout the world's oceans, contributing to the passive organic particle flux in highly variable fractions (0-100%)[5].

Copepods transport carbon actively by conducting daily vertical migrations (DVMs) and seasonal migrations. Zooplankton feeding in the surface layer at night, and seeking refuge at depth during the day leads to DVM[6] (Fig. 1a). Such migrations are widespread and most beneficial when food availability and predation pressure in surface waters are high, particularly for larger organisms that swim faster and more efficiently[7]. During daily vertical migrations, carbon consumed near the sea surface is respired and defecated at depth[8,9]. The magnitude of this form of carbon transport ranges up to 70% of passive organic particle fluxes[7] and reaches a few hundred meters of depth at maximum[10].

Copepods conduct seasonal vertical migrations to hibernate at depth[11], typically descending hundreds to thousands of meters. This strategy is found in polar and subpolar environments with severe winters. In the North Atlantic it is a conspicuous behavior in three *Calanus* species[12]. Carbon transport through seasonal migration results from respiration and mortality at depth (Fig. 1b). In regions where hibernating *Calanus* species are highly abundant, the magnitude of this process is comparable to passive organic particle flux[13–15].

Results and Discussion

We used an optimal behavior model[7] to estimate the extent of DVM for copepods observed by the Continuous Plankton Recorder (CPR) program[16,17] during the period 1960-2014. Optimal behavior models assume that the behavior of naturally selected organisms is optimal with respect to evolutionary fitness, and thus predictable if the effects of environmental characteristics on fitness are known (see Methods). Observations were taken at approximately 7 m depth and include adults, near-adults, and early life stages when available, of the 45 taxa comprising >99% of the biomass sampled (Supplementary Table 1). DVM depth and duration were estimated for each taxon based on food availability, temperature, light intensity, and body size. On the community level, we forced DVM duration to match observed differences in day- and night-time biomass (Supplementary Figure 3). The resulting DVM depth estimates varied within a conservative but realistic[10] range (Supplementary Figure 4).

From these DVM estimates, we derived fecal pellet and DVM fluxes out of the upper mixed layer. We assumed that copepods produce fecal pellets in response to feeding in the surface layer, and that copepod body size determines pellet size, and thus sinking velocity and flux attenuation[4]. DVM flux was estimated as the sum of fecal pellets released during

84 migration[7] and respiration below the local mixed layer . Furthermore, we accounted for the
85 effect of local temperature on feeding, respiration and remineralization rates (see Methods).

86 Spatiotemporal interpolations of fecal pellet and DVM fluxes at local mixed layer
87 depth showed distinct spatial patterns and a strong seasonal signal (Fig. 2). High flux areas
88 included the northwestern North Atlantic around the mouth of the Labrador Sea (Fig. 2a,b),
89 where copepod biomass and average body size were high (Supplementary Figure 5). Fecal
90 pellet fluxes were also high in the northern European and eastern North American shelf seas,
91 despite considerably smaller average body size. In the North Sea, for example, the large
92 population size of small copepods (Supplementary Figure 5) compensated for high
93 remineralization loss caused by slow average fecal pellet sinking velocity[18]. Integrated over
94 the entire area, carbon transport through sinking fecal pellets and DVM peaked in July, and
95 had a second, smaller peak in September (Fig. 2c). Flux timing in the open ocean followed a
96 south-north gradient, reaching 50% of total annual flux in May at 40°N, and about 2 months
97 later at 60°N (Fig. 2d). In shallow, coastal areas with ample food and a high fraction of the
98 copepod community hatching from resting eggs (Supplementary Figure 5), median annual
99 flux was reached even later (July to August).

100 From 1960 to 2014 distinct changes in fecal pellet and DVM fluxes occurred across
101 large parts of the study area. These fluxes have increased along the northern and northwestern
102 boundary from Iceland to the Gulf of Maine, and have decreased across much of the open
103 northern North Atlantic and the European Shelf Seas (Fig. 3a,b). During the past two
104 decades, net primary production has also increased at high latitudes (Supplementary Figure
105 10), due to warming and reduced sea ice coverage[19,20]. However, the spatial patterns of these
106 changes were not strongly linked to changes in flux (see Supplementary Results). Trends in
107 seven focal areas with high sampling effort highlight the spatial variability of change in

fluxes over the time series (Fig. 3c, d). We found distinct negative trends in the sum of the two fluxes in the areas "Iceland" and "Celtic S", while in the area "North S" the trend was slightly positive (Fig. 3c, d). Interestingly, the trends were linked to changes in the timing of 50% annual flux, with earlier timings being associated with decreasing annual fluxes. Overlaying the general trend, flux changes also showed considerable small-scale variation in magnitude and sometimes direction (Fig. 3a,b). Potentially, this variability resulted from the patchy distribution of copepod populations and it may have been amplified by the heterogeneous response of plankton species distributions to climate change[19,21,22] and consequent trophic mismatches[23].

We estimated the duration of seasonal migrations and abundance of migrating populations for the hibernating species *Calanus finmarchicus*, *C. hyperboreus*, and *C. glacialis* from spatiotemporal interpolations of night-time observations, and used them to calculate hibernation fluxes (respiration and mortality during overwintering), which we assumed to be restricted to areas of at least 500 meters depth (see Methods). Significant hibernation fluxes were confined to the northwestern half of the investigated area, peaking around the mouth of the Labrador Sea (Fig. 4a). This pattern resembled the distribution of *C. finmarchicus*, the most abundant of the hibernating species. The changes in hibernation fluxes between 1960 and 2014 were similar to those of fecal pellet and DVM fluxes, showing an increase along the northwestern boundary of the investigated area and a decrease further southeast. However, the area of hibernation flux increase was somewhat larger, including the focal area "Iceland" (Fig. 4c). In contrast to the general trend, hibernation fluxes declined during the most recent period in the "Labrador" and "Irminger" regions. This may ultimately be linked to changes in the distribution of *C. finmarchicus* populations, which have been related to large scale hydroclimatic oscillations, such as the North Atlantic Oscillation

(NAO), that control ocean currents and in turn the advection of the species[24]. Indeed the NAO Index was particularly low during the period 2004-2014, a condition that has been related to enhanced intrusion of subarctic water into the Scotian Shelf/Gulf of Maine region and associated declines in local *C. finmarchicus* populations[24].

Based on the flux estimates presented here, fecal pellet production represents the most important form of carbon transport by surface-layer copepods (Supplementary Figure 6). At mixed layer depth, fecal pellet flux was on average about ten times higher than DVM flux with highest relative differences in the shelf seas, where the fraction of migrating biomass was low, and in the southern part of the investigated area, where organisms were smaller and tended to remain at shallower depths (Supplementary Figures 4, 5). At 500 meters depth, the magnitudes of mean fecal pellet flux (including the contribution of abundant juvenile taxa) and mean hibernation flux (ignoring the contribution of juveniles) were similar. Hibernation flux transported more carbon to depth along the northwestern boundary of the study area, while fecal pellet flux dominated in the other parts.

We performed a sensitivity analysis to assess which of the temporally-resolved model inputs (i.e., copepod biomass, total abundance and abundance of key species, body size and temperature) most influenced the observed changes in carbon fluxes. Overall, changes in biomass correlated most strongly with changes in the fluxes modeled, with abundant, large-bodied species playing a key role (Fig. 5). A strong link between copepod biomass and carbon transport likely also exists for the poorly understood but potentially significant contributions from sinking carcasses and shed exoskeletons[3]. In contrast to the high spatiotemporal variations of biomass, mean copepod body size showed modest variability (Supplementary Figures 5, 7), and overall its temporal changes correlated less with changes in modeled carbon fluxes (Fig. 5). However, the relative importance of changes in body size

156 increased for fecal pellet fluxes estimated at greater depths. The distributions of *C.*
157 *finmarchicus* and *C. hyperboreus* are known to have shifted in response to climate change[25].
158 The significant positive correlations between their relocations and shifts in the modeled
159 carbon fluxes (Fig. 5) highlight how strongly relocations of dominant species can affect the
160 climate system.

161 The correlations between changes in copepod biomass and changes in flux
162 magnitudes were consistently positive across all focal areas at the $p \leqslant 0.01$ level (Fig. 5),
163 while the relationships of changes in sea surface temperature and body size with flux changes
164 were more variable in space. Links between flux changes and changes in sea surface
165 temperature were positive overall, as expected from our temperature-dependent formulation
166 of feeding and metabolic rates, but in several focal areas, this relationship was not found.
167 This result is not surprising as while increasing temperature has a direct, positive effect on
168 copepod metabolism, it is often associated with stratification-driven nutrient limitation and
169 smaller community body size[3] that have negative effects on community production and
170 carbon export[26]. In the "Labrador" region, where changes in fluxes show a close positive link
171 to changes in body size, decreasing community size structure during warm periods may have
172 compensated for flux increases from enhanced metabolism, or, as in the case of mixed layer
173 fecal pellet fluxes, even changed the sign to significant negative relationships between
174 temperature changes and flux changes

175 While the spatial and temporal *patterns* identified here can be considered
176 representative, our surface layer-based estimates of flux *magnitudes* are far smaller than those
177 of depth-integrated assessments. Globally, zooplankton fecal pellets may constitute 40% of
178 passive organic particle fluxes[3] and at high latitudes copepods may transport even more

carbon through seasonal migrations[13–15]. Our estimated total contribution of surface-layer copepods was 0.2 gC m^{-2} y^{-1} at mixed layer depth which is much less than the estimated 29 gC m^{-2} y^{-1} removed by the biological pump in the North Atlantic[2]. This is not surprising, as we only investigated the contribution of copepods in the top 14 meters, for which we considered our observational data to be representative. Consequently, for example our estimates of overwintering *C. finmarchicus* populations in the Labrador Sea were 53 times lower than hibernating populations counted at depth[13]. Nevertheless, the spatiotemporal patterns we identified in the surface waters are indicative for the layers below, as most taxa have connected populations spreading over wide depth ranges[27]. In the future, depth-integrated estimates of the zooplankton contribution to biogenic carbon flux may be enabled by increasingly available data from *in-situ* imaging surveys[28].

The biological pump is the result of the complex interplay of biological, chemical, and physical processes and is currently not understood sufficiently well to derive clear expectations of its response to future climate change[29,30]. Even modeling the comparably well-understood contribution of surface-layer copepods required several limiting assumptions that we discuss in depth in the Supplementary Discussion. One key uncertainty, for instance, comes from copepod coprophagy – the feeding on fecal pellets with complex effects on their remineralization and sinking behavior[5]. While we implicitly included coprophagy through an observation-based formulation of fecal pellet remineralization rates, we could not account for its spatiotemporal variability. We therefore examined to what extent coprophageous taxa (*Oithona* and *Oncaea*)[5] may affect spatial patterns in surface-layer fecal pellet concentration and, hence, flux (see Supplementary Results). As the concentration of sinking fecal pellets was considerably lower than the concentration of phytoplankton, unselective feeding on pellets vs phytoplankton may have reduced fecal pellet concentration only little, with the

greatest impacts in shelf seas and in the southern oceanic part of the study area (Supplementary Figure 9). As expected, coprophagy had the least impact in areas with high fluxes and large mean community body size. Given current knowledge, it is not possible to estimate the contribution of integrated zooplankton coprophagy on fecal pellet fluxes.

In summary, we used a complex, mechanistic modeling framework combined with an unparalleled long-term dataset to study the key pathways by which surface-layer copepods transport carbon to depth, and found robust and significant north-westward shifts in North Atlantic carbon fluxes, driven by changes in biomass distributions and copepod community structure. While the northern North Atlantic has the highest data coverage, future research should also investigate other hotspots of zooplankton carbon export, such as the Nordic Seas[13,14] and the Southern Ocean[15]. Building on the trait-based approach and evolutionary rationale, our modeling framework has the generality to be readily applied in such systems. Moreover, it can be incorporated into next-generation biogeochemical models to formalize the fluxes through size-structured representations of zooplankton communities, ultimately reducing the uncertainty of climate prognoses.

Methods

Overview

The analyses consisted of three steps: first we estimated fecal pellet fluxes, DVM fluxes, and hibernation fluxes using mechanistic models and spatiotemporal interpolation techniques; second, we analyzed various spatial and temporal summary statistics from these estimates; finally, we investigated the role of potential drivers of the temporal flux changes observed.

We used the same framework to estimate fecal pellet and DVM fluxes, and estimated hibernation fluxes separately. Fecal pellet and DVM flux estimates were based on an optimal behavior model assessing the trade-off between feeding opportunity and predation risk for copepods in the surface layer. Copepods were assumed to have the choice between feeding in the surface layer and hiding in deeper, darker layers where predation risk gets increasingly lower. We assumed copepods to choose to migrate until the marginal energetic costs for swimming and lost feeding opportunity level off with the marginal gain from lower mortality - the behavior yielding highest expected fitness. The larger a copepod, the more efficiently it feeds[31] and swims[7] and thus the deeper and longer it can afford to migrate. From the optimal behavior estimates, fecal pellet and DVM fluxes were estimated individually for each taxon and observation, summed up, and interpolated in space and time.

Calanus finmarchicus, *C. hyperboreus* and *C. glacialis* are the main species conducting seasonal hibernation in the North Atlantic. To quantify the carbon fluxes originating from this behavior, we first produced monthly abundance climatologies for each combination of hibernating species and 11-year period investigated by interpolating

observations in space and time. Then, we used these climatologies to derive the abundance of migrating individuals as well as the duration of their diapause. Finally, we estimated hibernation fluxes as the sum of respiration and mortality at depth, integrated over the duration of the diapause. Respiration rates were assumed to depend on local temperature and on the body size of the organisms[14].

Spatially resolved estimates for fecal pellet-, DVM-, and hibernation-fluxes – in the former two cases with additional seasonal resolution - were produced for five eleven-year periods. From these estimates we calculated annual means, total magnitude, phenology as well as decadal trends. Finally, we investigated how decadal trends in the flux estimates are linked to changes in temperature, copepod biomass, total copepod abundance and abundance of important taxa, and mean community body size. All analyses were conducted in the R environment[32].

Data

Copepod community observations

We used Continuous Plankton Recorder (CPR) observations from 1960 to 2014 amounting to over 219,000 observations of 45 copepod taxa resolved in abundance classes[17] (Supplementary Table 1). Observed life stages comprised adults and copepodites V. For *Calanus*, *Metridia*, *Paracalanus* and *Pseudocalanus* species, younger copepodite stages were also included.

We analyzed temporal trends of carbon fluxes based on five periods by splitting the observational data into the subsets 1960-1970, 1971-1981, 1982-1992, 1993-2003, and 2004-2014. The spatial extent of the analyses was confined to the area of regular CPR sampling,

263 which we defined as pixels with a low standard deviation of spatiotemporal interpolations
264 (see below). Furthermore, we defined seven focal areas with high sampling frequency for in-
265 depth analyses (see Figs. 3, 4 and 5). These areas encompassed 8000 km^2 (except "Central A"
266 covered 32,000 km^2) and were of rectangular shape with an aspect ratio of 2:1 when mapped
267 in geographic space. The areas "North S", "Celtic S", and "Newfoundl." were shallower than
268 500 meters and therefore not in the area of expected hibernation fluxes. The vertical extent of
269 the study included the top 14 m of the water column, for which we assumed the CPR samples
270 (taken at about 7 m depth) to be representative[4].

271 ***Environment***

272 In order to estimate carbon fluxes, we needed information on temperature, food
273 availability, water turbidity, and the depth of the mixed layer. For temperature (*T*) we used
274 data from both the World Ocean Atlas[33] and the Hadley Centre for Climate Prediction and
275 Research[34]. Data from the World Ocean Atlas consist of six roughly decadal climatologies
276 covering the periods 1955-1964, 1965-1974, 1975-1984, 1985-1994, 1995-2004, and 2005-
277 2012, with 1°×1° horizontal resolution, and a vertical resolution of 5 and 25 m for 0-100 and
278 100-500 m depth, respectively. Temperatures in the years 2013 and 2014 were approximated
279 with the most recent climatology. We used local polynomial regression fitting to derive
280 smooth local depth profiles for the optimal behavior models, and assumed the November-to-
281 February averages of local temperature at 500 meters to represent the conditions experienced
282 during hibernation at depth. In order to obtain accurate estimates of temperature changes
283 throughout the study period, we also used the annually resolved sea surface temperature
284 product HadISST1 from the Hadley Centre (1°×1° horizontal resolution).

285 Food availability was approximated based on phytoplankton biomass. We used size-
286 resolved phytoplankton biomass estimates[35] to account for the fact that copepods cannot

directly feed on pico-phytoplankton. Phytoplankton biomass available to copepods was assumed to include microplankton and nanoplankton plus one tenth of the estimated picoplankton biomass. The latter term was included because 10% of the picoplankton biomass may be assimilated by heterotrophic flagellates, on which copepods can feed. We used an average monthly climatology of available phytoplankton biomass that was based on the years 1997 to 2010 and aggregated to 0.5°×0.5° horizontal resolution. Water turbidity was represented by the diffuse attenuation coefficient of the downwelling irradiance at 490 nm (KD490) as available on the GlobColour website (http://www.globcolour.info/). We aggregated the monthly estimates from 1998 to 2014 to produce a climatology with 0.25°×0.25° horizontal resolution. For mixed layer depth (*MLD*) we used one monthly 0.5°×0.5° climatology to cover all observations[36]. Elevation data, used to constrain areas suitable for seasonal dormancy and to illustrate topography in the maps, was derived from the ETOPO1 Global Relief Model[37].

Copepod dimensions

To estimate migration behavior and carbon fluxes, we needed information on copepod body size. We compiled data on prosome length (*PL*), prosome width, and aspect ratio (η) from various sources (Supplementary Table 1), and computed copepod volume (*V*) as[38]

$$V = \frac{4}{3}\,\pi\,(\frac{PL}{2})^3\,\eta^2 \quad (1)$$

and carbon mass (m_c) from the empirical relationship[31]

$$log(m_c) = -0.93 + 0.95 \times log(m_w) \quad (2)$$

where m_w is wet mass which we estimated assuming a copepod density of 1 g cm^{-3}. For a few species, information on aspect ratio was not available and estimated based on information from other taxa considered (see Supplementary Table 1 for details).

Statistics

We used statistics to constrain our mechanistic carbon flux models with data, to interpolate variables in space and time, to investigate temporal trends, and to investigate links between decadal changes in fluxes and potential drivers. To this end we employed spatiotemporal models, linear regression, quantile regression, and hypothesis testing.

Spatiotemporal interpolations

We made spatiotemporal interpolations using the Integrated Nested Laplace Approximation (INLA) approach to model the distribution of average DVM duration, carbon fluxes, biomass, abundance, and equivalent spherical radius. The INLA approach is a computationally-efficient, Bayesian statistical tool that is particularly powerful in handling spatial and spatiotemporal correlation structures[39,40]. We assumed the modeled distributions to be isotropic, stationary Gaussian Fields and used the Stochastic Partial Diferential Equation approach on discrete mesh points covering the investigated area (Supplementary Figure 1) for the interpolations. Furthermore, we exploited the seasonal autocorrelation in the data to produce well-informed climatologies. To this end, we assumed an autoregressive relation with the closest neighbors between the monthly time steps (AR1 process). A detailed description of the set-up of the spatiotemporal models is provided in the Supplementary Methods.

Regressions for temporal trends

We used linear regressions to estimate temporal trends in carbon fluxes over the periods investigated. Quantile regression was used to identify trend lines in for parameters that were resampled from a posterior distribution; otherwise simple linear regression was employed.

Hypothesis testing

Hibernating population and diapause duration

In order to estimate hibernation fluxes, we needed spatially-resolved information on the abundance of the hibernating individuals, as well as on the duration of their diapause. We obtained this information from the spatiotemporal interpolations of the abundance of the hibernating species. In order to estimate the duration of the diapause, a pixel-wise hypothesis-testing approach was employed.

The hibernating *Calanus* species are known to have diapause durations that vary in space. *C. finmarchicus* has been observed to be hibernating between four and seven months[13], while the maximum hibernation duration for *C. hyperboreus* ranges up to eight months[14]. From this information we assumed *C. finmarchicus* and, due to its similar size, *C. glacialis* to be hibernating between four and seven months, and *C. hyperboreus* between five and eight months. Furthermore, we assumed that diapause always included the months December and January. These constraints reduced the realm of possible monthly dormancy periods for the species to either 18 or 22 options (e.g., five months duration beginning in September, six months duration beginning in October, etc.). We treated these options as hypotheses and tested them by fitting simple linear models to pixel-wise seasonal abundance data, assuming diapause periods and feeding seasons to differ in mean copepod abundance in the surface layer. The most probable dormant period was assumed to be the one for which the corresponding model had the lowest Akaike information criterion (AIC) value. Once the most probable diapause period was identified, the abundance of hibernating copepods was estimated: we assumed a staggered onset of seasonal migration with individuals of a number

equivalent to the current surface-layer population descending during each of the last three feeding season months.

Correlations in changes of decadal trends

We used two-sided correlation tests to estimate strength and significance of correlations between decadal changes in carbon fluxes and changes in variables feeding into the carbon flux models, including sea surface temperature, community mean equivalent spherical radius, copepod biomass, copepod abundance, and abundance of important copepod taxa. Changes were estimated pixel-wise on a 1°×1° grid and between all consecutive periods. Pearson correlation tests were used when both variables tested were interpolated with the same error distribution, otherwise Spearman correlation tests were used.

Mechanistic models

Modelling fecal pellet and DVM fluxes

Estimates of fecal pellet fluxes and DVM fluxes were based on a recently published optimal behavior model[7] that we complemented with three major aspects: we considered the effects of temperature through temperature-dependent formulations of metabolic rates; we forced DVM duration to match empirical estimates at the community level; and we also modeled carbon export through fecal pellets during the time copepods spend feeding at the surface.

Optimal migration behavior model

The model[7] assumes a copepod faces a common trade-off between acquiring energy for growth and reproduction and avoiding predation. This trade-off can be formalized by

Gilliam's rule[41] which defines optimal behavior as that which maximizes net energy gain divided by mortality rate. In the context of DVM, the optimal behavior may be defined as a function of the depth of migration (z_{max}) and the fraction of day spent migrating (τ):

$$f(z_{max}, \tau) = \frac{\varepsilon_{assim} g(z_{max},\tau) - c(z_{max},\tau)}{\mu(z_{max},\tau)} \quad (3)$$

where g is the total energy consumed (J d^{-1}) and ε_{assim} the assimilation efficiency: we assume that the food consumed by copepods is channeled to equal parts into catabolic metabolism (growth) (ε_{gr}), anabolic metabolism (ε_{resp}) where it is ultimately respired, and into defecation (ε_{fec}). The assimilation efficiency is the sum of the former two channels ($\varepsilon_{assim} = \varepsilon_{gr} + \varepsilon_{resp} = 2/3$). c is the energetic cost of the behavior (J d^{-1}) and μ is the mortality rate (d^{-1}). We define the total energy gain (g) as a function of the amount of food taken up divided by the relative metabolic day length

$$g(z_{max}, \tau) = \beta e_p (1 - \tau) \times \frac{1}{d_m(z_{max},\tau)} \quad (4)$$

where the coefficient e_p is the energy content of the prey (J gC^{-1}), 1-τ is the fraction of the day spent feeding, and β is the feeding rate (gC d^{-1}). We assume that feeding rate depends on body mass and temperature and has a linear relationship with food availability up to a threshold defined by maximum ingestion rate

$$\beta = \min(a_c(m_c) m_c c_p Q_{10}^{\frac{(15-T_{z0})}{10}}, a_i(m_c) m_c Q_{10}^{\frac{(15-T_{z0})}{10}}) \quad (5)$$

where $a_c(m_c)$ and $a_i(m_c)$ are empirical, mass-dependent estimates of mass-specific clearance rate and maximum ingestion rate, respectively, at a reference temperature[31] of 15 °C. m_c is copepod body mass (g C), and c_p is the available phytoplankton biomass (g m^{-3}). The parameter Q_{10} is the factor by which metabolic rates change for a temperature change of 10 °C, which we assumed to be 2.8. Finally, T_{z0} is the temperature at grazing depth

(°C).where $a_c(m_c)$ and $a_i(m_c)$ are empirical, mass-dependent estimates of mass-specific clearance rate and maximum ingestion rate, respectively, at a reference temperature[31] of 15 °C. m_c is copepod body mass (g C), and c_p is the available phytoplankton biomass (g m^{-3}). The parameter Q_{10} is the factor by which metabolic rates change for a temperature change of 10 °C, which we assumed to be 2.8. Finally, T_{z0} is the temperature at grazing depth (°C).

The relative metabolic day length (d_m) in equation (4) is estimated as the base metabolic activity experienced when migrating to deeper, cooler layers relative to the expected base activity when staying at the surface:

$$d_m(z_{max}, \tau) = (1 - \tau) + \tau Q_{10}^{-(T_{zmax} - T_{z0})/10} \quad (6)$$

whereby T_{zmax} is the temperature at migration depth (°C). By considering the metabolic day length, resting phases at cool temperatures are rewarded, as they allow a more efficient consumption of the energy taken-up.

The other two terms needed to estimate optimal migration behavior (Eq. 3) are mortality (μ) and cost (c). Many pelagic predators, for example fish, use visual cues to detect their prey, and we therefore assume predation mortality to depend on light exposure. Light exposure changes with migration depth, but also with water turbidity, time of the day, season and latitude. We approximated local turbidity with remotely sensed estimates of the extinction coefficient of irradiance at 490 nm wave length (KD490) and assumed an elevated mortality factor of 50 to obtain realistic migration depths[10] (see ref. [7] for details).

The cost of migrating arises from the energy demands for swimming. Swimming costs depend on the size of the copepods - as large organisms are more efficient swimmers than

small organisms – and they are proportional to the squared swimming velocity which depends on the migration depth (see ref. [7] for details).

Determining the optimal migration behavior

The frame-work formulated above provides a strong mechanistic reasoning for size-dependent differences in DVM behavior of different individuals. However, the assumption that predation risk is only a function light intensity ignores spatiotemporal variations imposed by factors like predator abundance, which are more difficult to quantify. In order to still account for such spatiotemporal variations, we forced modeled behaviors to match our empirical estimates of DVM duration on the community level. To this end we fixed average DVM duration when we sample-wise optimized for the migration durations and depths of the observed taxa which yield the highest mass-weighted mean fitness. A detailed description of the optimization procedure is given in the Supplementary Methods.

Carbon export from fecal pellets

We assumed that fecal pellets are produced in response to feeding with a delay of 30 min gut transit time[42]. We estimated the fecal pellet fluxes individually for each taxon in a sample as the amount of pellets produced that did not remineralize before they have reached the vertical boundary (mixed layer depth or 500 meters depth),

$$Flux_{fecal,i} = \frac{FPCP_i}{RR+SR_i/h}\frac{\tau_{opt,i}-t_t}{\tau_{opt,i}} e^{(-RR/\,SR_i)(z_0-z_b)} SR_i n_i \quad (7)$$

where z_b is the depth of the vertical boundary and z_0 is grazing depth. SR_i (m d^{-1}) is the fecal pellet sinking rate which depends on fecal pellet volume and ultimately copepod prosome length[4]. We assume that *SR* decreases with depth as remineralization continuously reduces the volumes of the pellets. *RR* represents specific remineralization rate (d^{-1}) which we

assumed to be temperature-dependent. h is the thickness of the surface layer; t_t represents gut transit time; and n is the abundance of the observed taxon i. $FPCP_i$ is the fecal pellet carbon production (gC m^3 d^{-1}) estimated as

$$FPCP_i = \mathrm{g}\left(z_{max,opt,i}, \tau_{opt,i}\right) d_m\left(z_{max,opt,i}, \tau_{opt,i}\right) \varepsilon_{fec} \frac{1}{e_p} \quad (8)$$

with g being the energy gain at optimal migration behavior, d_m the relative metabolic day length, $1/e_p$ the energy to carbon ratio, and ε_{fec} the defecated fraction of the carbon consumed. A description of the depth-dependent calculation of remineralization loss is given in the Supplementary Methods.

Carbon export from daily vertical migration

We define the carbon export through daily vertical migration as the fraction of daily respiration that happens below the mixed layer plus one stomach volume of fecal pellets released at migration depth:

$$Flux_{resp,i} = g\left(z_{max,opt,i}, \tau_{opt,i}\right) \frac{1}{e_p} \varepsilon_{resp} \tau_{ML,i} Q_{10}^{-(T_{zmax} - T_{z0})/10} n_i h + \frac{FPCP_i}{RR + SR_i/h} \frac{t_t}{\tau_{opt,i}} e^{(-RR/SR_i)(z_{max,opt,i} - MLD)} SR_i n_i \quad (9)$$

Here, g is the energy gain from the optimal behavior; $1/e_p$ the energy to carbon ratio; ε_{resp} is the respired fraction; and $\tau_{ML,i}$ is the fraction of day spent below the mixed layer. The Q_{10}-term describes the relative reduction of respiration due to the temperature difference at depth analogously to Eq. 6; n represents the abundance of individuals of taxon i; and h is the thickness of the representative surface layer. The second term is analogous to the fecal pellet flux, except that remineralization loss only takes place from the maximum migration depth to

MLD, and that the excreted amount only corresponds to one stomach volume, which we estimate as one gut transit time of grazing. An overview over the parameters and constants used to estimate fecal pellet and DVM fluxes is given in Supplementary Table 2.

Modelling hibernation fluxes

We estimated carbon fluxes for each of hibernating species individually before summing them up. Three main processes contribute to carbon fluxes through copepods in diapause below the permanent thermocline: respiration, mortality and expiring females - females which end their life cycles at depth in spring after having released their eggs[14]. Visser et al. (ref. [14]) propose a general form to estimate these terms for dormant copepod species:

$$Flux_{hiber,i} = \sum_{stage} n_i \frac{(1-e^{-\mu_i D_i})}{\mu_i D_i} r_i D_i + \sum_{stage} n_i (1 - e^{-\mu_i D_i}) \left(m_i + w_{i,max} - \frac{r_i D_i}{2}\right) + \xi n_F e^{-\mu_F D_F} \left(m_F + w_{F,max} - r_F D_F - C_{egg}\right) \quad (10)$$

where *stage* are the dormant life stages, *n* is abundance at the beginning of the dormancy period, and *D* is the duration of the dormancy period. μ is mortality, which we assume to be 0.001 d^{-1} (ref. [14]). *m* and *w* are structural and reserve mass, respectively, which can be estimated based on their relationship with the prosome length (see ref. [14]). *r* is the respiration rate which is a function of the body size of the dormant life stage, as well as the local temperature (see ref. [14]) which we represented with temperature data at 500 m depth. ξ is the fraction of females that expire at depth, which is one for *Calanus hyperboreus* and zero for *C. finmarchicus*, and *C. glacialis*. We assumed adult females to represent 25% of the hibernating *Calanus* taxa sampled by the CPR, as these classes contain both copepodite V life stages and adults, as well as both sexes. Finally, C_{egg} is the amount of carbon invested in egg production, assumed to be 900 µgC.

Availability

Data

Data generated to support the findings of this study are available within the paper and its supplementary information files.

Code

All analyses were conducted in the R environment[32]. Maps were created with the software Generic Mapping Tools[43]. Code generated for analyses and mapping is available from the corresponding author upon reasonable request.

References

1. Sigman, D. M. & Boyle, E. A. Glacial/interglacial variations in atmospheric carbon dioxide. *Nature* **407,** 859–869 (2000).

2. Sanders, R. *et al.* The Biological Carbon Pump in the North Atlantic. *Prog. Oceanogr.* **129,** 200–218 (2014).

3. Steinberg, D. K. & Landry, M. R. Zooplankton and the Ocean Carbon Cycle. *Ann. Rev. Mar. Sci.* **9,** 413–444 (2017).

4. Stamieszkin, K. *et al.* Size as the master trait in modeled copepod fecal pellet carbon flux. *Limnol. Oceanogr.* **60,** 2090–2107 (2015).

5. Turner, J. T. Zooplankton fecal pellets, marine snow, phytodetritus and the ocean's biological pump. *Prog. Oceanogr.* **130,** 205–248 (2015).

6. Hays, G. C. Zooplankton avoidance activity. *Nature* **376,** 650–650 (1994).

7. Hansen, A. N. & Visser, A. W. Carbon export by vertically migrating zooplankton: an optimal behavior model. *Limnol. Oceanogr.* **61,** 701–710 (2016).

8. Steinberg, D. K. *et al.* Zooplankton vertical migration and the active transport of dissolved organic and inorganic carbon in the Sargasso Sea. *Deep Sea Res. Part I Oceanogr. Res. Pap.* **47,** 137–158 (2000).

9. Al-Mutairi, H. & Landry, M. R. Active export of carbon and nitrogen at Station ALOHA by diel migrant zooplankton. *Deep Sea Res. Part II Top. Stud. Oceanogr.* **48,** 2083–2103 (2001).

10. Ohman, M. D. & Romagnan, J.-B. Nonlinear effects of body size and optical attenuation on Diel Vertical Migration by zooplankton. *Limnol. Oceanogr.* **61,** 765–770 (2016).

11. Dahms, H. U. Dormancy in the Copepoda - an overview. *Hydrobiologia* **306,** 199–211 (1995).

12. Brun, P., Payne, M. R. & Kiørboe, T. A trait database for marine copepods. *Earth Syst. Sci. Data* **9,** 99–113 (2017).

13. Jónasdóttir, S. H., Visser, A. W., Richardson, K. & Heath, M. R. Seasonal copepod lipid pump promotes carbon sequestration in the deep North Atlantic. *Proc. Natl. Acad. Sci. U. S. A.* **112,** 12122–6 (2015).

14. Visser, A. W., Grønning, J. & Jónasdóttir, S. H. Calanus hyperboreus and the lipid pump. *Limnol. Oceanogr.* **62,** 1155–1165 (2017).

15. Bradford-Grieve, J. M. Potential contribution that the copepod Neocalanus tonsus makes to downward carbon flux in the Southern Ocean. *J. Plankton Res.* **23,** 963–975 (2001).

16. Richardson, A. J. *et al.* Using continuous plankton recorder data. *Prog. Oceanogr.* **68,** 27–74 (2006).

17. Johns, D. G. Raw data for copepods in the North Atlantic (25-73N, 80W-20E) 1960-2014 as recorded by the Continuous Plankton recorder. (2016). doi:10.7487/2016.250.1.1007

18. Beaugrand, G., Edwards, M. & Legendre, L. Marine biodiversity, ecosystem

functioning, and carbon cycles. *Proc. Natl. Acad. Sci.* **107,** 10120–10124 (2010).

19. Sundby, S., Drinkwater, K. F. & Kjesbu, O. S. The North Atlantic Spring-Bloom System—Where the Changing Climate Meets the Winter Dark. *Front. Mar. Sci.* **3,** (2016).

20. Martinez, E., Antoine, D., D'Ortenzio, F. & de Boyer Montégut, C. Phytoplankton spring and fall blooms in the North Atlantic in the 1980s and 2000s. *J. Geophys. Res.* **116,** C11029 (2011).

21. Chivers, W. J., Walne, A. W. & Hays, G. C. Mismatch between marine plankton range movements and the velocity of climate change. *Nat. Commun.* **8,** 14434 (2017).

22. Poloczanska, E. S. *et al.* Global imprint of climate change on marine life. *Nat. Clim. Chang.* **3,** 919–925 (2013).

23. Edwards, M. & Richardson, A. J. Impact of climate change on marine pelagic phenology and trophic mismatch. *Nature* **430,** 881–4 (2004).

24. Greene, C. & Pershing, A. J. The response of Calanus finmarchicus populations to climate variability in the Northwest Atlantic: basin-scale forcing associated with the North Atlantic Oscillation. *ICES J. Mar. Sci.* **57,** 1536–1544 (2000).

25. Chust, G. *et al.* Are Calanus spp. shifting poleward in the North Atlantic? A habitat modelling approach. *ICES J. Mar. Sci.* **71,** 241–253 (2013).

26. Cermeño, P. *et al.* The role of nutricline depth in regulating the ocean. *Proc. Natl. Acad. Sci. U. S. A.* **105,** 20344–20349 (2008).

553 27. Palomares-Garcia, R. J., Gomez-Gutierrez, J. & Robinson, C. J. Winter and summer
554 vertical distribution of epipelagic copepods in the Gulf of California. *J. Plankton Res.*
555 **35,** 1009–1026 (2013).

556 28. Guidi, L. *et al.* Plankton networks driving carbon export in the oligotrophic ocean.
557 *Nature* **532,** 465–470 (2016).

558 29. Boyd, P. W. Toward quantifying the response of the oceans' biological pump to
559 climate change. *Front. Mar. Sci.* **2,** 1–15 (2015).

560 30. Intergovernmental Panel on Climate Change. in *Climate Change 2014 Impacts,*
561 *Adaptation, and Vulnerability* (eds. Field, C. B., Barros, V. R., Dokken, D. J., Mach,
562 K. J. & Mastrandrea, M. D.) 411–484 (Cambridge University Press, 2014).
563 doi:10.1017/CBO9781107415379.011

564 31. Kiørboe, T. & Hirst, A. G. Shifts in Mass Scaling of Respiration, Feeding, and Growth
565 Rates across Life-Form Transitions in Marine Pelagic Organisms. *Am. Nat.* **183,**
566 E118–E130 (2014).

567 32. R Core Team. R: A Language and Environment for Statistical Computing. (2013).

568 33. Locarini, R. A. *et al. World Ocean Atlas 2013, Volume 1: Temperature*. (NOAA Atlas
569 NESDIS 73, 2013).

570 34. Rayner, N. A. *et al.* Global analyses of sea surface temperature, sea ice, and night
571 marine air temperature since the late nineteenth century. *J. Geophys. Res.* **108,** 4407
572 (2003).

573 35. Kostadinov, T. S., Milutinović, S., Marinov, I. & Cabré, A. Carbon-based

phytoplankton size classes retrieved via ocean color estimates of the particle size distribution. *Ocean Sci.* **12,** 561–575 (2016).

36. Schmidtko, S., Johnson, G. C. & Lyman, J. M. MIMOC: A global monthly isopycnal upper-ocean climatology with mixed layers. *J. Geophys. Res. Ocean.* **118,** 1658–1672 (2013).

37. Amante, C. & Eakins, B. W. *ETOPO1 1 Arc-Minute Global Relief Model: Procedures, Data Sources and Analysis*. (NOAA Technical Memorandum NESDIS NGDC-24. National Geophysical Data Center, 2009). doi:10.7289/V5C8276M

38. Jiang, H. & Kiorboe, T. The fluid dynamics of swimming by jumping in copepods. *J. R. Soc. Interface* **8,** 1090–1103 (2011).

39. Rue, H., Martino, S. & Chopin, N. Approximate Bayesian inference for latent Gaussian models by using integrated nested Laplace approximations. *J. R. Stat. Soc. Ser. B (Statistical Methodol.* **71,** 319–392 (2009).

40. Blangiardo, M. & Cameletti, M. *Spatial and Spatio-temporal Bayesian Models with R-INLA*. (Wiley, 2015).

41. Gilliam, J. F. & Fraser, D. F. Habitat Selection Under Predation Hazard: Test of a Model with Foraging Minnows. *Ecology* **68,** 1856–1862 (1987).

42. Kiørboe, T. & Tiselius, P. T. Gut clearance and pigment destruction in a herbivorous copepod, Acartia tonsa , and the determination of in situ grazing rates. *J. Plankton Res.* **9,** 525–534 (1987).

43. Wessel, P., Smith, W. H. F., Scharroo, R., Luis, J. & Wobbe, F. Generic Mapping

595 Tools: Improved Version Released. *Eos, Trans. Am. Geophys. Union* **94,** 409–410
596 (2013).

Figures

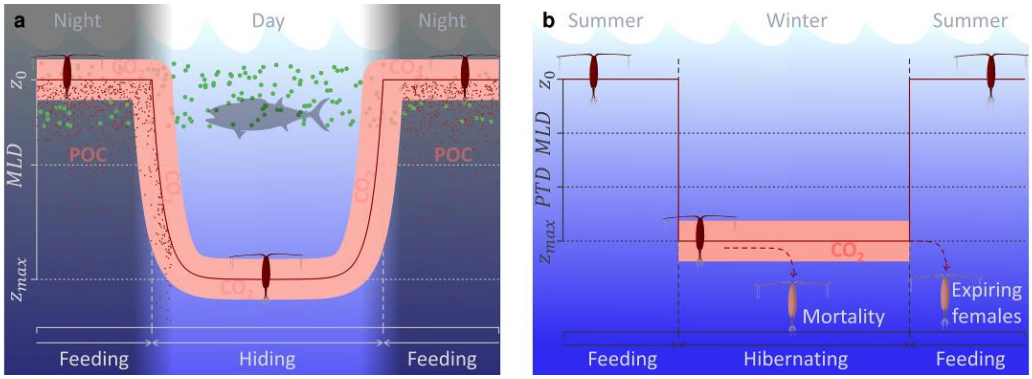

Figure 1: Schematic illustrations of daily and annual vertical distributions of copepods and associated carbon fluxes. Panel (a) shows carbon fluxes related to the daily vertical migration behavior (fecal pellet flux and DVM flux). Panel (b) illustrates seasonal hibernation below the permanent thermocline (PTD) and associated hibernation flux. MLD indicates mixed layer depth; POC represents particulate organic carbon.

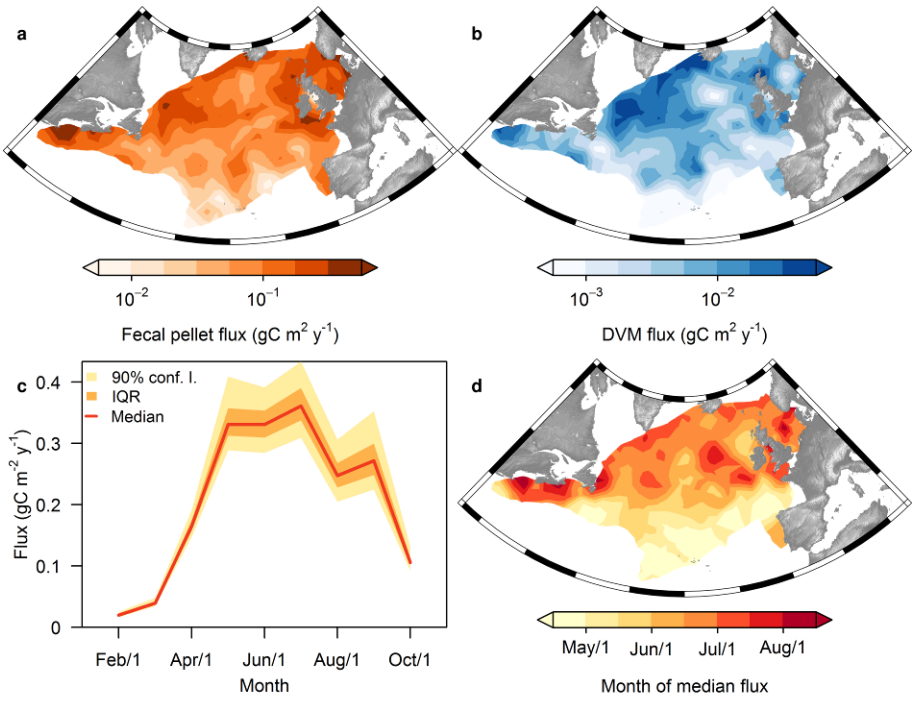

605

606 Figure 2: Distribution and phenology of fecal pellet and DVM fluxes at mixed layer
607 depth for the period 2004-2014. Distributions of annual averages are shown for fecal pellet
608 (a) and DVM fluxes (b). Monthly averages of their sum are shown in panel (c) where the red
609 line connects medians and orange and yellow polygons illustrate interquartile range and 90%-
610 confidence intervals, respectively. Panel (d) shows the distribution of the timing of 50%
611 annual flux. Estimates for November and January are lacking due to missing information on
612 food availability (considered zero for averaging). Maps of interpolation uncertainty are
613 shown in Supplementary Figure 8.

614

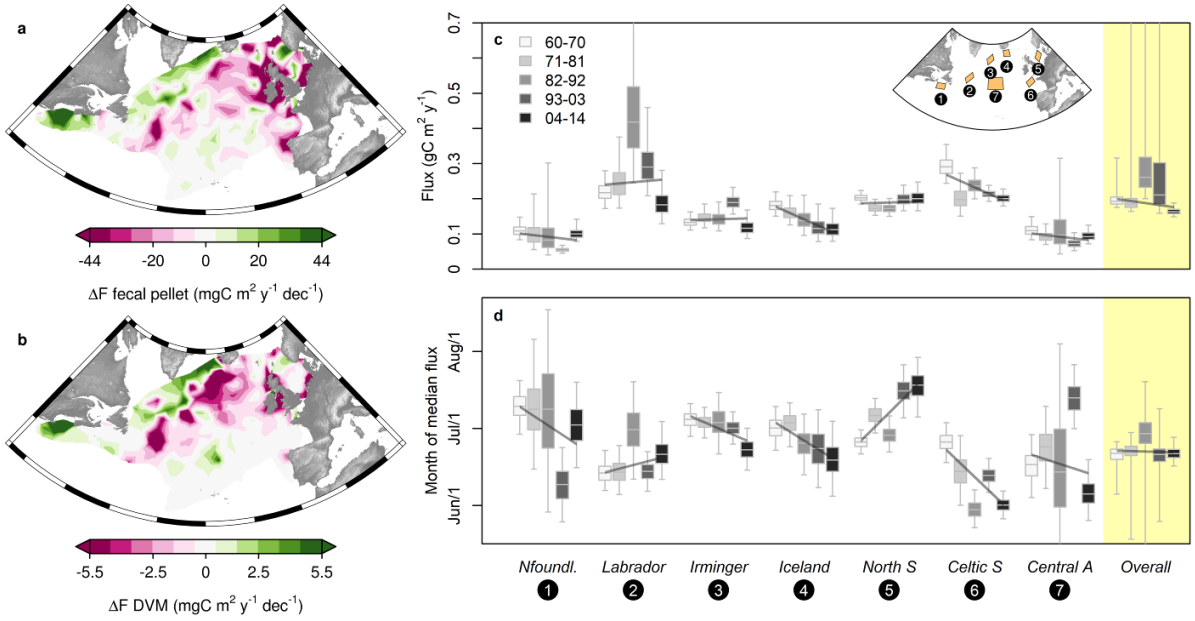

615

616 Figure 3: Trends in fecal pellet and DVM fluxes at mixed layer depth from 1960 to
617 2014. Slopes of linear regressions between flux estimates and time are shown for fecal pellet
618 fluxes (a) and DVM fluxes (b) at mixed layer depth. Decadal estimates of annual flux (c) and
619 timing of 50% annual flux (d) are shown with uncertainty from spatiotemporal interpolations
620 for the entire study area and seven focal areas. Central lines in boxplots illustrate medians,
621 boxes illustrate interquartile ranges and whiskers represent 95%-confidence intervals.
622 Superimposed trend lines illustrate changes in medians.

623

624 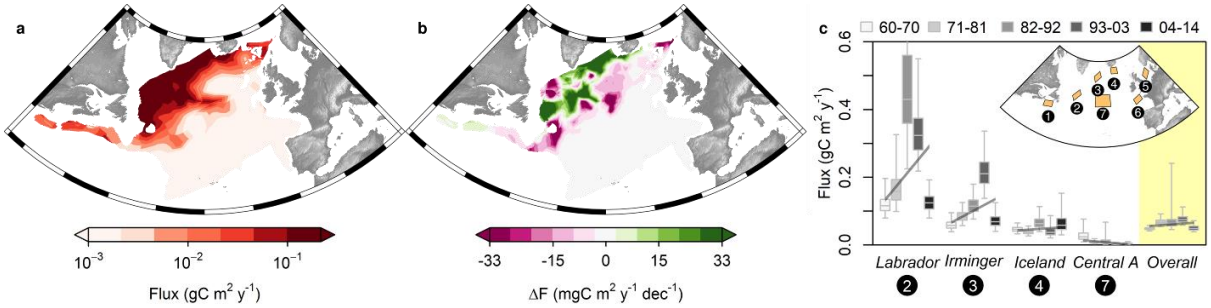

625 Figure 4: Distribution and trends in hibernation fluxes. Distributions for the period
626 2004-2014 are shown in panel (a). Slopes of linear regressions between flux estimates and
627 time are shown for the period 1960 to 2014 in panel (b). For focal areas deeper than 500m
628 periodical estimates are shown with uncertainty (c). Central lines in boxplots illustrate
629 medians, boxes illustrate interquartile ranges and whiskers represent 95%-confidence
630 intervals. Superimposed trend lines illustrate changes in medians.

631

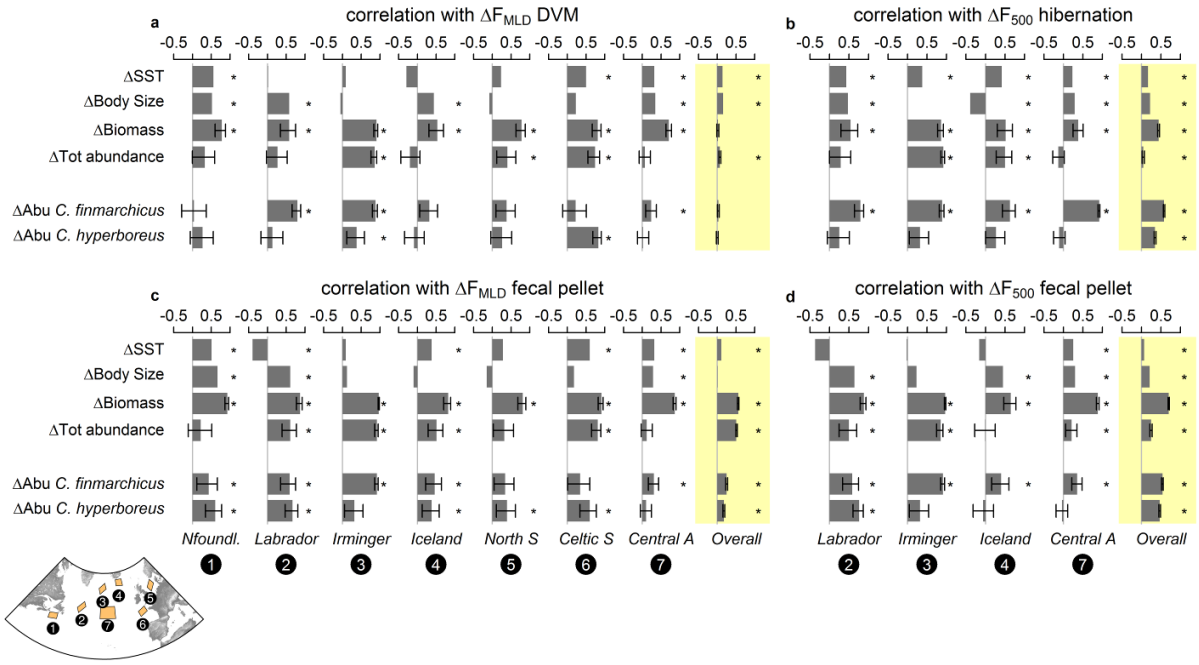

632

633 Figure 5: Correlation coefficients between flux changes and changes in key variables
634 feeding into the models. Depicted are relationships of DVM flux at mixed layer depth (a),
635 hibernation flux at 500 m (b), fecal pellet flux at mixed layer depth (c), and fecal pellet flux at
636 500 m (d), with sea surface temperature, body size, biomass, and abundance. Correlation
637 coefficients were estimated for the entire study area and seven focal areas. Error bars indicate
638 95%-confidence intervals and asterisks indicate significance at the $p \leqslant 0.01$ level. For
639 correlations between carbon fluxes and sea surface temperature or body size we used
640 Spearman correlation, otherwise Pearson correlation. Correlations with abundance of
641 additional taxa are shown in Supplementary Results.

642

Supplementary information

Pdf files:

Supplementary Information

Acknowledgements

We acknowledge the Villum foundation for support to the Centre for Ocean Life. Further support was received from the Gordon & Betty Moore Foundation through award #5479' (TK and AVW), the NSF GRFP grant #DGE-1144205 (KS), and the European Union 7th Framework Programme (FP7 2007–2013) through grant agreement number 308299 (NACLIM) (MRP). Finally, we wish to thank the many current and retired scientists at SAHFOS whose efforts over the years helped to establish and maintain the Continuous Plankton Recorder survey, and Hans van Someren Gréve for the beautiful copepod illustration.

Author contributions

PB, KS, AWV, MRP and TK designed the study. KS developed the fecal pellet model. PL selected the taxa used and compiled the data. PB performed the analysis and prepared the manuscript with contributions and support from the other authors.

Competing interests

The authors declare no competing financial interests.

Supplementary Information

to the paper "Climate change has altered zooplankton-fuelled carbon export in the North Atlantic"

Supplementary Methods

Dimensions of copepod taxa considered

Supplementary Table 1: Taxa considered in this study as sampled by the Continuous Plankton Recorder and their estimated dimensions, including prosome length (*PL*), prosome width (*PW*), aspect ratio ($\eta = PW/PL$), body volume (V), equivalent spherical radius (r), and carbon mass (m).

CPR taxon	*PL* (mm)	*PW* (mm)	η	V (mm^3)	r (mm)	m (mg C)
Oncaea spp.	0.54**	0.19	0.35§	0.01	0.13	0.01
Oithona spp.	0.79	0.27*	0.34*	0.03	0.19	0.01
Acartia spp. (unidentified)	1.00	0.33*	0.33*	0.06	0.24	0.03
Mecynocera clausi	1.01	0.36*	0.36*	0.07	0.25	0.03
Isias clavipes	1.03¶	0.36	0.35§	0.07	0.26	0.03
Calocalanus spp.	1.09	0.39*	0.36*	0.09	0.27	0.04
Corycaeus spp.	1.09	0.43*	0.39*	0.11	0.29	0.05
Para-Pseudocalanus spp.	1.39	0.44*	0.32*	0.14	0.32	0.06
Clausocalanus spp.	1.29	0.47*	0.36*	0.15	0.33	0.06
Centropages hamatus	1.39	0.52*	0.37*	0.20	0.36	0.08
Scolecithricella spp.	1.40	0.52*	0.37*	0.20	0.36	0.09
*Cal*anus I-IV	1.65	0.50*	0.30*	0.22	0.37	0.09
Centropages bradyi	1.45¶	0.54	0.37‡	0.22	0.38	0.09
Centropages spp. (Unidentified)	1.51	0.56††	0.37††	0.25	0.39	0.11
Temora longicornis	1.30	0.62*	0.48*	0.26	0.40	0.11
Metridia I-IV	1.66	0.60*	0.36*	0.31	0.42	0.13
Labidocera wollastoni	1.73¶	0.60	0.35§	0.33	0.43	0.14
Centropages typicus	1.69	0.63*	0.37*	0.35	0.44	0.15
Mesocalanus tenuicornis	1.79	0.64*	0.36*	0.38	0.45	0.16
Pleuromamma borealis	1.99	0.73*	0.37*	0.56	0.51	0.23
Pleuromamma gracilis	1.99	0.73*	0.37*	0.56	0.51	0.23
Nannocalanus minor	2.00	0.74*	0.37*	0.57	0.52	0.23
Calanoides carinatus	2.40	0.75*	0.31*	0.71	0.55	0.28
Metridia longa	2.3⋆	0.83	0.36*	0.84	0.58	0.33
Calanus helgolandicus	2.80	0.81*	0.29a	0.96	0.61	0.38
Anomalocera patersoni	2.55¶	0.89	0.35§	1.06	0.63	0.42
Pleuromamma V-VI (Trav)	2.56‡‡	0.94	0.37§§	1.18	0.66	0.46
Metridia Total traverse	2.60‖‖	0.94	0.36‖‖	1.21	0.66	0.47
Candacia armata	2.60	1.00*	0.38*	1.36	0.69	0.53
Calanus finmarchicus	2.99	0.95*	0.32*	1.41	0.70	0.55
Subeucalanus crassus	3.12	0.95*	0.30*	1.47	0.71	0.57
Paraeuchaeta hebes	2.91	1.04*	0.36*	1.65	0.73	0.63
Metridia lucens	2.90	1.05*	0.36*	1.67	0.74	0.64
Neocalanus gracilis	3.21	1.07*	0.33*	1.92	0.77	0.73
Euchirella rostrata	3.01	1.14*	0.38*	2.05	0.79	0.78
Heterorhabdus norvegicus	2.99	1.15*	0.38*	2.07	0.79	0.79
Calanus glacialis	3.57‖	1.08	0.30†	2.18	0.80	0.83
Pleuromamma abdominalis	3.49	1.28*	0.37*	3.00	0.89	1.12
Rhincalanus nasutus	5.02	1.14*	0.23*	3.41	0.93	1.27
Undeuchaeta plumosa	3.71	1.33*	0.36*	3.44	0.94	1.27
Euchaeta acuta	3.81	1.36*	0.36*	3.69	0.96	1.36
Pleuromamma robusta	3.99	1.46*	0.37*	4.45	1.02	1.63
Pleuromamma xiphias	4.59	1.68*	0.37*	6.78	1.17	2.43
Calanus hyperboreus	6.40#	1.94	0.30†	12.57	1.44	4.37
Paraeuchaeta norvegica	7.50	2.68*	0.36*	28.22	1.89	9.42

673 * values obtained from refs. [2] and [3]; † average of corresponding values for *Calanus finmrachicus* and *Calanus helgolandicus*; ‡ average of
674 corresponding values for *Centropages typicus* and *Centropages hamatus*; § average of corresponding values for all taxa considered; ‖ values
675 obtained from ref. [4]; ¶ values estimated as 0.75 × mean total length, as reported by ref. [5]; # value obtained from ref. [6]. ⋆ Value obtained from
676 http://www.arcodiv.org/. ** average of *Oncaea media*, *Oncaea mediterrana* and *Oncaea venusta* as obtained from ref. [7]. †† average of
677 *Centropages* species considered. ‡‡ value obtained from ref. [8]. §§ average of *Pleuromamma* species considered. ‖‖ Average of *Metridia* species
678 considered.

679 ## Spatiotemporal model design

680 ### *Average DVM duration*

681 The average duration of daily vertical migration was estimated based on the CPR
682 observations and used to constrain the optimal behavior estimates (see below). We calculated
683 a DVM index (*DVM**) of the following form:

684 $$DVM^* = \frac{bm_n - bm_d}{bm_n} \quad \text{(S1)}$$

685 where *bm* is mean biomass at night or day[3]. For each observation we first estimated
686 biomass (mgC m^{-3}) of the present copepods, and determined whether it was made at night or
687 during daylight hours. Then, we interpolated bm_n and bm_d observations from the entire data
688 set, using the ILNA approach with default priors and assuming zero-inflated, negative
689 binomial error distributions. As *DVM** is based on the ratio between two interpolated fields
690 with negative binomial error distributions, it is particularly susceptible to gaps in the
691 observational data. We accounted for this vulnerability by interpolating on a coarse, discrete
692 spatial mesh with 375 points (Supplementary Figure 1), and by simultaneously fitting bm_n
693 and bm_d using the spatiotemporal effect of the night-time observations as an additional,
694 stabilizing predictor for the day-time observations. In a few locations (on average 3% of the
695 area) the estimates of *DVM** went slightly below zero (i.e., more biomass during day time
696 than at night). We treated these cases as sampling errors and set *DVM** to zero, i.e., assuming
697 no migration. The average fraction of day spent migrating (τ_c) necessary for subsequent
698 analyses was then estimated by multiplying *DVM** estimates with the local relative day
699 length at the time of sampling.

Abundance, carbon fluxes, biomass, and equivalent spherical radius

We modeled the spatial distribution of copepod abundance, carbon fluxes, copepod biomass, and mean equivalent spherical radius of copepods using default priors and a relatively fine spatial mesh with 1552 points (Supplementary Figure 1) and considered only observations made during night time (106,907 observations), when we assumed the entire community to be present. For fecal pellet and DVM fluxes the seasonal resolution did not include winter months (November to January) where satellite data on available phytoplankton biomass and water turbidity was not available for high latitudes (76,439 observations). Community-weighted mean equivalent spherical radius was estimated as the carbon mass-weighted mean of the radii of the taxa present[11]. We assumed zero-inflated, negative binomial error distributions for abundance, carbon fluxes and biomass, while normal distribution was assumed for the error of equivalent spherical radius estimates.

Uncertainty assessment

One strength of estimating spatiotemporal interpolations with the INLA approach is that full uncertainty information is estimated. In the SPDE approach in INLA, for each mesh point (Supplementary Figure 1) not single values are provided but posterior probability distributions. The width of these probability distributions thereby depends on the number of local data points, their variability, and - if the standard deviation of the chosen error distribution family is a function of its mean - magnitude. These estimated probability densities allow the generation of replicate maps by resampling values for each mesh point and subsequent interpolation. We resampled 1000 such maps for uncertainty assessment, and used them to recalculate the quantities of interest. From these samples we derived uncertainty maps (Supplementary Figure 8) and estimated the regional medians and confidence intervals reported in the boxplots of Figs. 3c,d and 4c.

Spatial meshes used in INLA

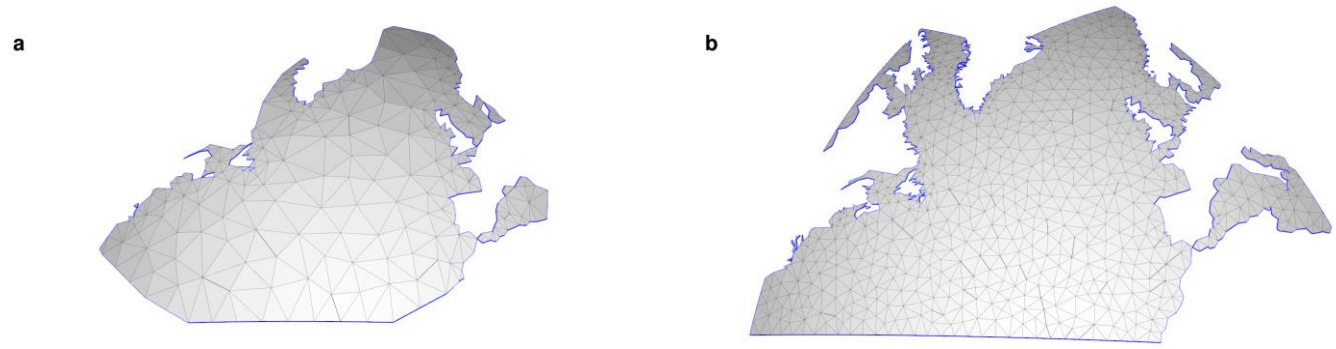

Supplementary Figure 1: Delaunay-triangulated mesh used to estimate the spatial dependencies in INLA models. Panel (a) shows a crude mesh containing 375 vertices that is used to model daily vertical migration; Panel (b) shows a fine mesh containing 1552 vertices that is to model carbon fluxes, biomass, abundance, and body size (see Supplementary Methods). We projected the coordinates onto a sphere in order to realistically represent the spatial relationships.

Constants and parameters used to model fecal pellet and DVM fluxes

Supplementary Table 2: Overview over constants and parameters used to model fecal pellet and DVM fluxes

Parameter	*Description*	*Value*	*Unit*
f	Fitness		J
g	Gain from grazing		J d^{-1}
μ	Total mortality*		d^{-1}
c	Cost of migration*		J d^{-1}
τ	Fraction of day spent migrating		-
z_{max}	Maximum migration depth		m
z_0	Grazing depth	7	m
z_b	Depth of the vertical boundary		m
ε_{assim}	Assimilation efficiency	2/3	-
ε_{resp}	Respired fraction of carbon intake	1/3	-
ε_{fec}	Defecated fraction of carbon intake	1/3	-
ε_{gr}	Carbon intake invested in growth	1/3	-
e_p	Energy content of prey	4200	J gC^{-1}
β	Maximum feeding rate		m^3 d^{-1}
$a_c(m_c)$	Specific clearance rate scaling at 15°C†		m^3 g C^{-1} d^{-1}
$a_i(m_c)$	Specific maximum ingestion rate scaling at 15°C†		g C g C^{-1} d^{-1}
t_t	Gut transit time	1/48	d
d_m	Relative metabolic day length		-
Q_{10}	Magnification of vital rates of active copepods at 10 °C increase	2.8	-
$FPCP$	Fecal pellet carbon production		gC m^3 d^{-1}
SR	Fecal pellet sinking rate		m d^{-1}
RR	Remineralization rate		d^{-1}
h	Thickness of surface layer	14	m
m_c	Mass of copepod		g C
r	Radius of copepod		m

T	Temperature	°C
n	Copepod abundance	ind m^{-3}
c_p	Available phytoplankton biomass	g m^{-3}
MLD	Mixed layer depth	m

* Parameter specified in ref. [9]; † Parameter specified in ref. [10]

Optimizing daily vertical migration behaviors

The optimization procedure employed consisted of two steps which will be illustrated at the example of CPR sample „8NA-25“ (Supplementary Figure 2). This sample was taken at the mouth of the Labrador Sea in August of 1963, and contained the taxa *Oithona* spp., *Calanus* copepodites, and *Paraeuchaeta norvegica.* There was a significant thermal gradient in the top 70 meters, and roughly average food availability and water turbidity (Supplementary Figure 2a-e). In a first step we summarized the relative fitness for each taxon present and the given environmental conditions as a function of τ and z_{max}. We discretized the range of τ into 50 steps and derived optimal fitness and corresponding z_{max} for each of these steps, using the univariate Brent optimization algorithm[12]. Next, we interpolated between these optimum points to obtain functional relationships between τ and optimal z_{max} as well as between τ and optimal relative fitness using local polynomial regression fitting (Supplementary Figure 2i-n).

In a second step we used the functional relationships between τ and optimal relative fitness to simultaneously determine the optimal migration behaviors of all taxa present in a sample. If more than one taxon was present in a sample we used the multidimensional Nelder-Mead optimization algorithm[13], chose the observed average DVM duration (derived from the local *DVM** value) as starting point for each taxon, and maximized mean fitness under the constraint that mass-weighted mean DVM duration remains constant. In addition, we penalized high variance among the fitness estimates for the different taxa in order to avoid low fitness estimates for rare taxa. The optimization argument was thus

$$\max\left(\frac{1}{\sum_i m_{c,i} n_i}\sum_i (f_i\, m_{c,i} n_i) - var(\boldsymbol{f})\right) \quad \text{(S2)}$$

where $m_{c,i}$ is the mass of taxon i, n_i its abundance and *var* is variance, while f_i and $\boldsymbol{f}$ are relative fitness for taxon i and for all taxa present, respectively.

Three types of functional relationships between τ and relative fitness were possible. Relative fitness could monotonously decrease with τ, as in the exemplary case of small *Oithona* spp. sample „8NA-25“ (Supplementary Figure 2l) – the optimal behavior of the taxon is thus to remain at the surface; relative fitness could be highest at τ=0 and reach a local minimum around τ=0.2 and a local maximum around τ=0.5, as in the exemplary case of intermediately-sized *Calanus* copepodites (Supplementary Figure 2m); or relative fitness could be highest around τ=0.5 and reach a local minimum close to τ=0.2, as in the exemplary case of large *P. norvegica* (Supplementary Figure 2n). The local minima in the latter two cases could cause optimization problems if the starting values and the global maxima were on opposite sides of them, i.e., if the optimization had to go through a local minimum to reach a global maximum. If this was the case, and the constraint on τ allowed for it, we adapted the starting values taxon-wise, and placed them in proximity of the global maxima. This adaptation was kept if it improved the optimization.

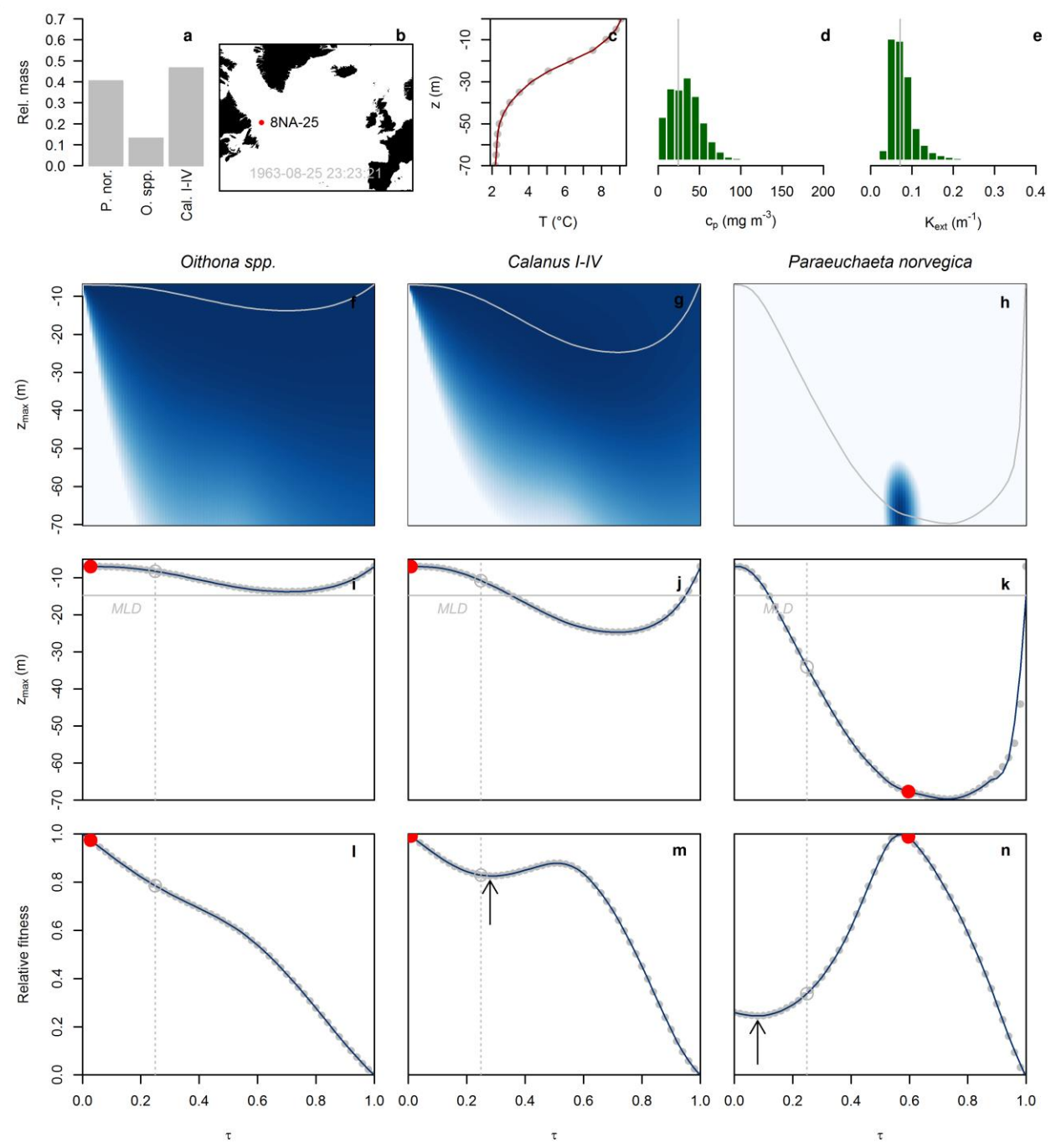

Supplementary Figure 2: Demonstration of optimization procedure at the example of CPR sample „8NA-25“. Relative mass of taxa present is shown in panel (a); map with the location of the sample is shown in panel (b); local temperature profile in the top 70 meters of the water column is shown in panel (c); available phytoplankton carbon concentration at the sample site relative to the frequency distribution across the study area shown in panel (d); light attenuation at the sample site relative to the frequency distribution across study area is shown in panel (e); relative fitness of the taxa present as a function of migration duration (τ) and migration depth (z_{max}) is shown in panels (f-h). Superimposed grey lines indicate migration depths of maximum fitness as a function of τ. Relationships between τ and z_{max} at optimal fitness and superimposed community optimization results are shown in panels (i-k). Horizontal grey lines indicate local mixed layer depth. Relationships between τ and optimal relative fitness with superimposed optimization results are shown in panels (l-n). In panels (i-n) grey dots represent optimal fitness (l-n) and corresponding z_{max} (i-k) for a given value of τ; dark blue lines are

interpolations between these points using local polynomial regression fitting; dotted, vertical lines represent observed average migration duration (based on *DVM**) which is used as initial value in the community optimization, and red points indicate optimization results. Arrows in panels (m) and (n) highlight local minima which may pose challenges to the optimization algorithm.

Remineralization rate

A general relationship between fecal pellet remineralization and temperature has not been established yet and was therefore estimated based on available information from the literature. Carbon-specific degradation rates for diatom aggregates have been measured[14] at 12 ± 3% at 15 °C, while they were 3.5 times lower at 4 °C. Similarly, at warmer temperatures remineralization in the field has been shown to be confined to shallower layers[15]. Also, a study[16] conducted in the Sargasso Sea indicates a 75% reduction in the remineralization of organic material between 150 and 500 m. From these estimates, we designed a specific remineralization rate based on a linear relationship with temperature:

$$RR = 0.005\,T + 0.011 \quad \text{(S3)}$$

where T is temperature (°C). This relationship provided remineralization rates that decreased exponentially with depth, in line with estimates from particulate organic carbon profiles[17,18].

Depth-dependent remineralization loss

Large fecal pellets sink faster than smaller pellets, and as pellets sink they lose volume through decomposition and remineralization. We explicitly modeled changes in both remineralization and fecal pellet sinking. To this end the depth range from the position of the copepod to the vertical boundary was divided into boxes that corresponded to the resolution of the temperature data (5-25 m). For each box the remineralization rate was estimated based on the local temperature. In addition, the local fecal pellet volume of each taxon present was

807 calculated by subtracting the volume lost while settling through the layers above from the
808 initial volume. From the local fecal pellet volume a local sinking rate was calculated. Local
809 remineralization rate and sinking rate were then used to calculate the remineralization loss
810 through the box.

Supplementary Results

Observed fraction of the migrating biomass (*DVM**)

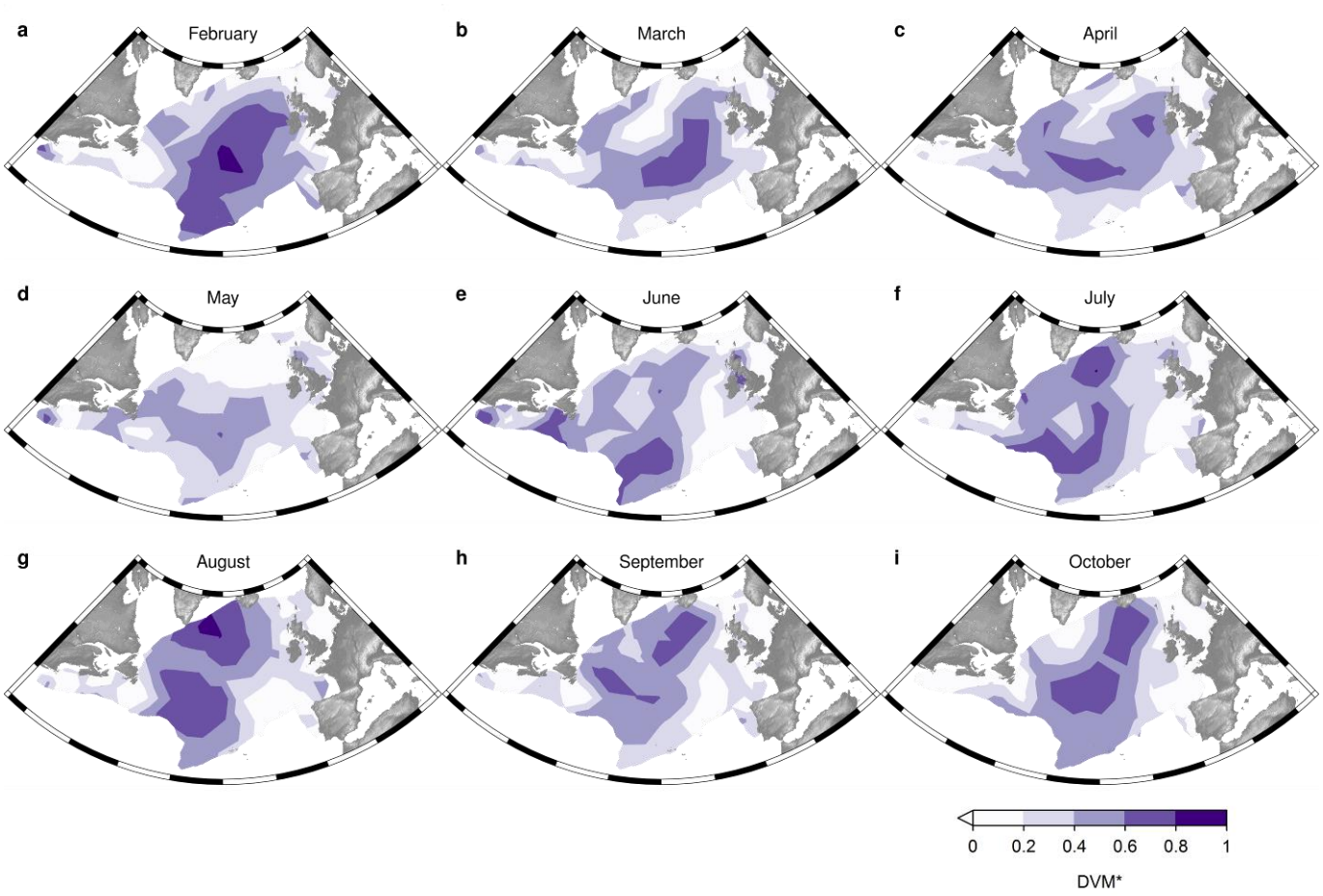

Supplementary Figure 3: Spatial distribution of the fraction of the migrating biomass (*DVM**) estimated as the fraction of night-time biomass that disappears during day-light hours (see Methods for details). Average *DVM** of the period 1960-2014 is shown for the months February to October (a-i).

Identified optimal daily vertical migration behaviors

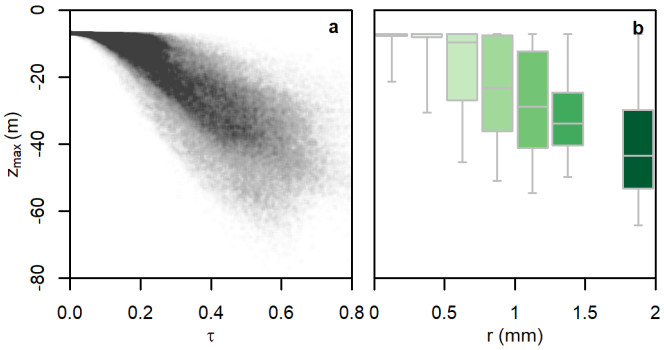

Supplementary Figure 4: Estimated values for migration depth (z_{max}) depending on fraction of day spent migrating (a) and body size (b) for all taxa and observations. τ represents fraction of day spent migrating and r is equivalent spherical radius of the organisms.

Distribution of relevant variables

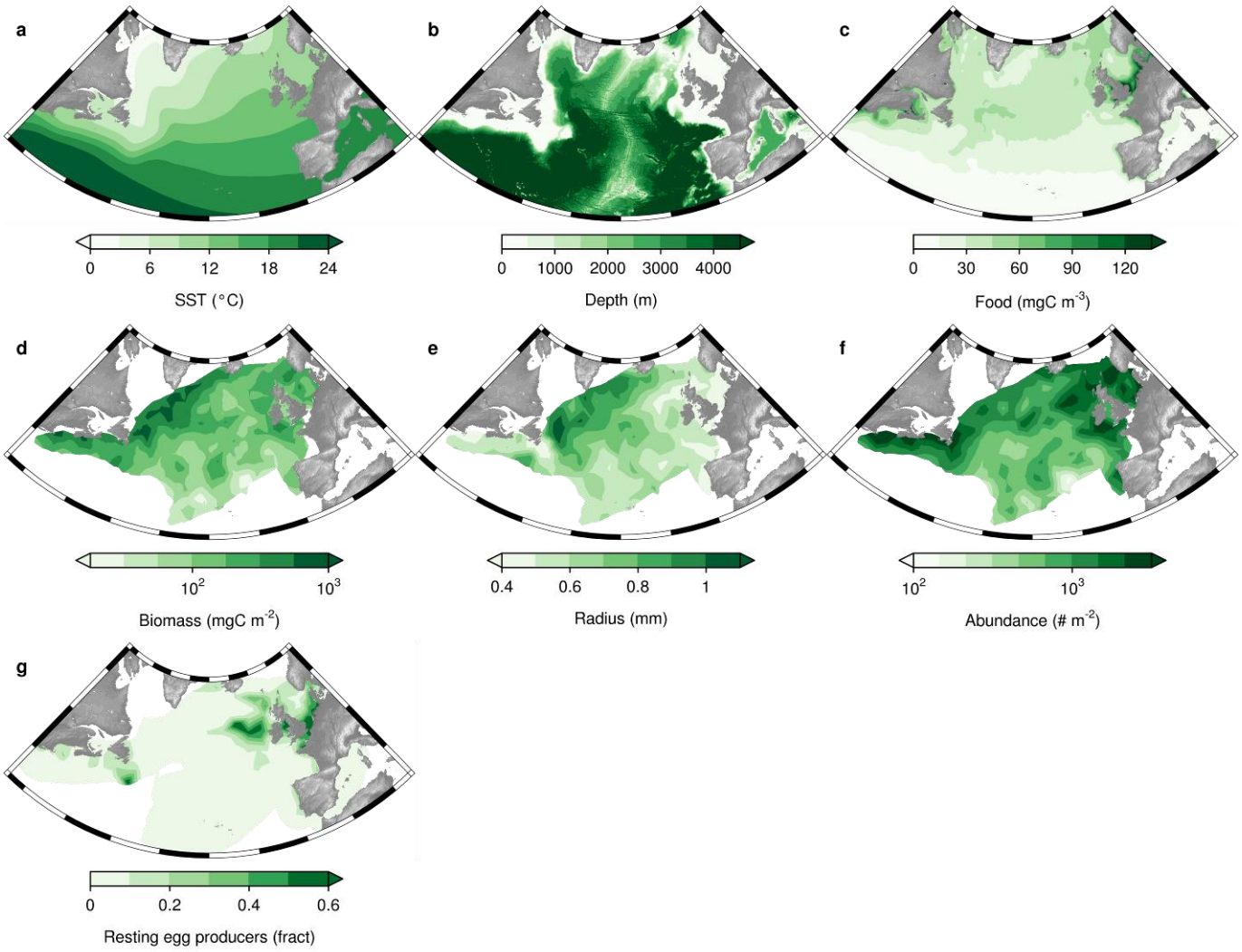

Supplementary Figure 5: Spatial distribution of variables with potential explanatory relevance. Illustrated are annual mean sea surface temperature (a), bathymetry (b), annual mean copepod food concentration (c), annual mean copepod biomass (d), annual mean prosome length (e), annual mean abundance (f), and annual mean of the weight fraction of resting egg producers (g). Distribution of weight fraction of resting egg producers is redrawn from ref. [1].

Relative importance of the different fluxes

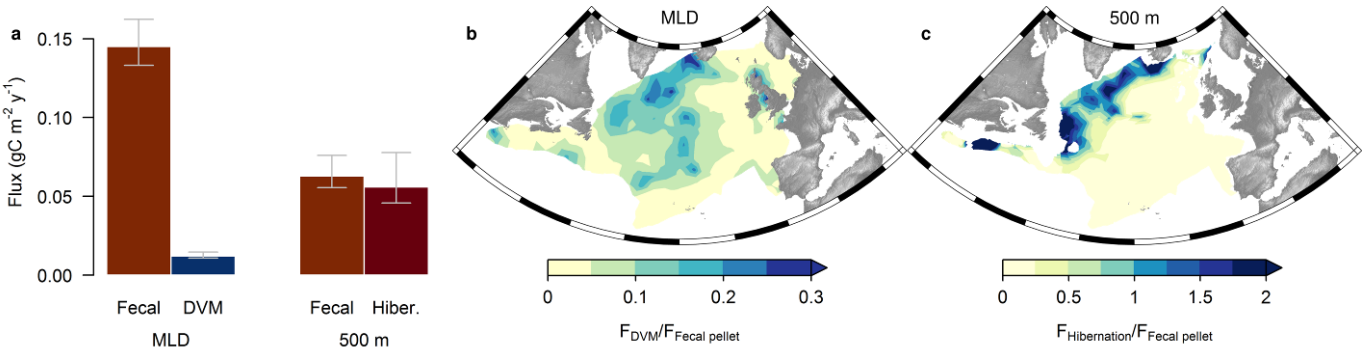

Supplementary Figure 6: Relative importance of the modeled carbon fluxes in the period 2004-2014. Total magnitude of fecal pellet and DVM fluxes at mixed layer depth and fecal pellet and hibernation fluxes at 500 m depth are shown in panel (a) where bars represent medians and error bars indicate 90% confidence intervals. Spatial distribution of ratios are shown for DVM and fecal pellet fluxes at mixed layer depth (b) and hibernation and fecal pellet fluxes at 500 m (c).

Decadal changes of potential predictors

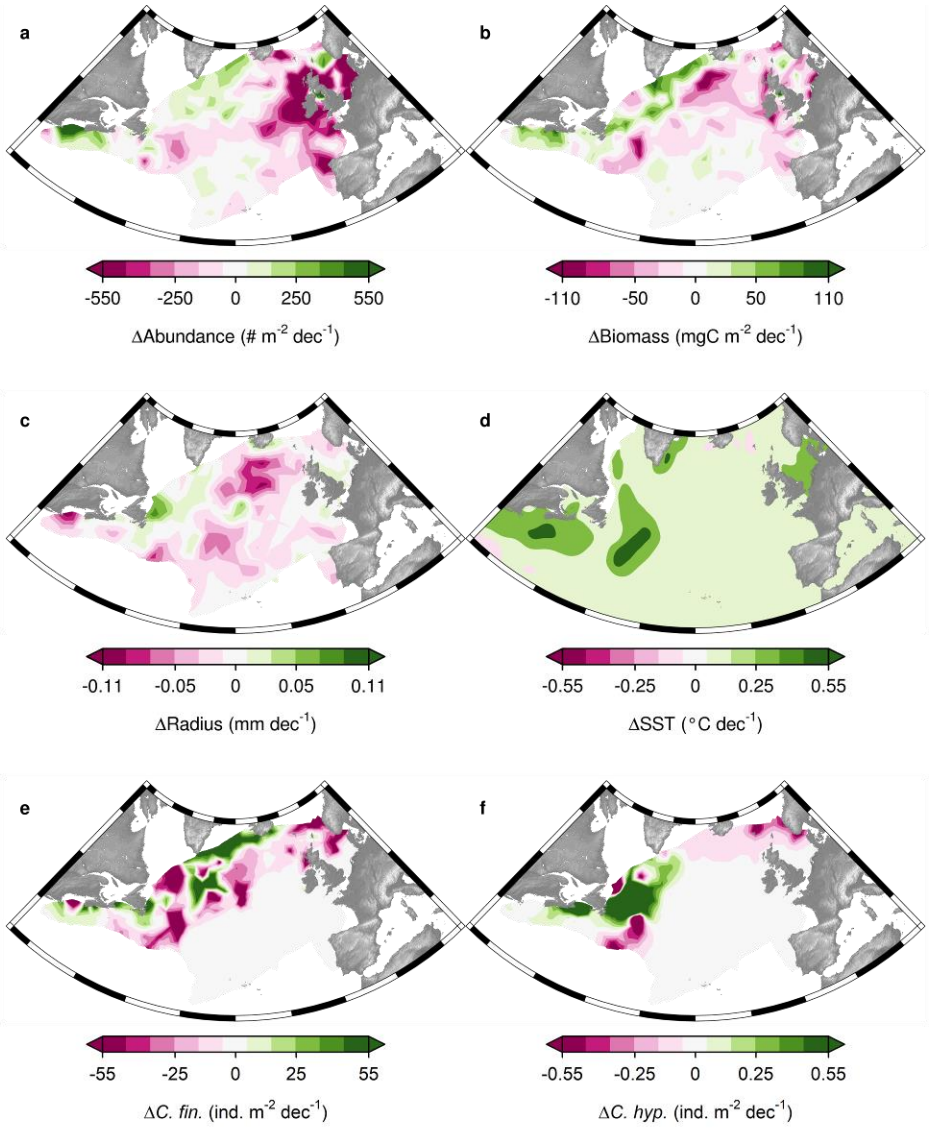

Supplementary Figure 7: Trends in potential predictors from 1960 to 2014. Illustrated are slopes of linear regressions between abundance (a), biomass (b), equivalent spherical radius (c), sea surface temperature (d), abundance of *C. finmarchicus* (e), abundance of *C. hyperboreus* (f), and time.

Detailed uncertainty maps

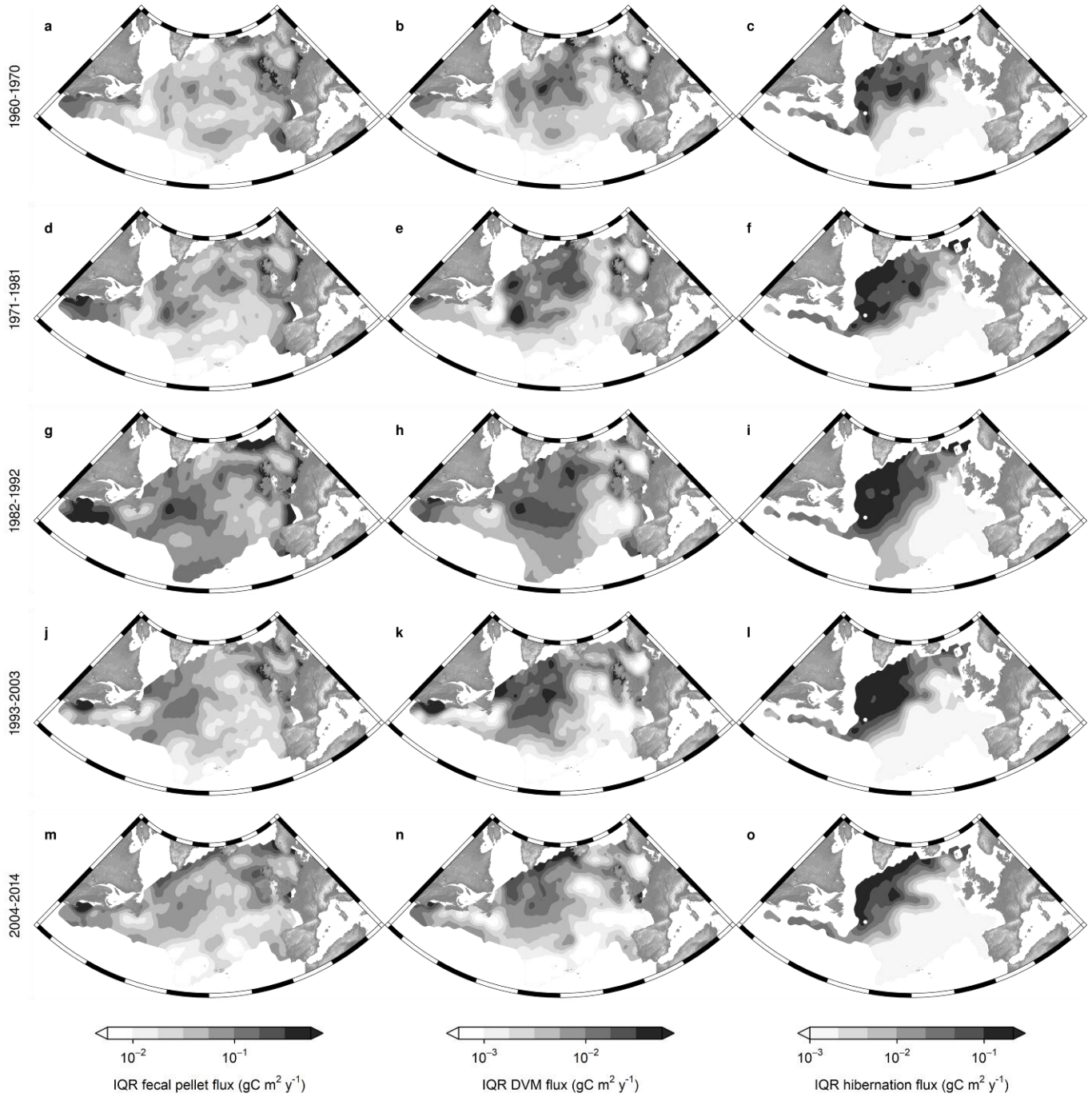

Supplementary Figure 8: Uncertainty maps for fecal pellet and DVM fluxes at mixed layer depth and for hibernation fluxes at 500 meters. Rows represent the periods considered. Uncertainty is represented as interquartile ranges estimated from 1000-fold resampling of flux/abundance maps. Uncertainty depends on sampling density, variability in observations, and mean abundance/flux, as for negative binomial distributions variance is a function of the mean.

Correlation coefficients between flux changes and abundance of further taxa

Supplementary Table 3: Correlation coefficients between flux changes and changes in sea surface temperature, body size, biomass, and abundance of an extended set of abundant taxa for the entire study area. Changes were estimated pixel-wise on a 1°×1° grid and between all subsequent periods. Subscripts indicate estimates at mixed layer depth or 500 meters. *Calanus* I-IV include pooled copepodite lifestages 1-4 of the four reported *Calanus* species. "Abu *Calanus* total" is the summed abundance of all reported *Calanus* classes.

	Corr. type	ΔF_{MLD} DVM	ΔF_{MLD} fecal pellet	ΔF_{500} fecal pellet	ΔF_{500} hibernation
ΔSST	Spearman	0.15*	0.12*	0.09*	0.17*
ΔBodysize	Spearman	0.24*	0.07*	0.27*	0.22*
ΔBiomass	Pearson	0.06*	0.6*	0.71*	0.44*
ΔTot abundance	Pearson	0.1*	0.48*	0.2*	0.05*
ΔAbu *C. finmarchicus*	Pearson	0.07*	0.29*	0.51*	0.58*
ΔAbu *C. hyperboreus*	Pearson	0	0.23*	0.5*	0.35*
ΔAbu *C. glacialis*	Pearson	0.03*	0.05*	0.08*	0.37*
ΔAbu *C. helgolandicus*	Pearson	0.05*	0.17*	0.07*	0.03
ΔAbu *Calanus* I-IV	Pearson	-0.05*	0.16*	0.11*	0.07*
ΔAbu *Calanus* total	Pearson	-0.01	0.26*	0.33*	0.32*
ΔAbu *Para-/Psuedocalanus*	Pearson	0.12*	-0.05*	-0.11*	0.12*

* correlation coefficient significantly different from zero, $p \leq 0.01$

Effect of surface-layer coprophagy on fecal pellet concentration

Among the abundant copepod taxa considered in this study *Oithona* spp. and *Oncaea* spp. have been observed to include fecal pellets in their diet, thereby contributing to fecal pellet flux attenuation in the epipelagic zone[19–21]. In a sensitivity analysis, we estimated the magnitude and spatial distribution of the fraction of surface-layer fecal pellet concentration potentially consumed by these organisms. To this end, we assumed the diet of *Oithona* and *Oncaea* to include both available phytoplankton biomass and fecal pellets of all studied copepod taxa but themselves, and no preference between these food sources. The food

concentration available to these taxa was therefore somewhat elevated, increasing their feeding rates but also their own fecal pellet production.

For each observation we estimated the potential fraction of surface-layer fecal pellets removed by *Oithona* and *Oncaea* coprophagy and made spatiotemporal interpolations for the period 2004-2014 using the INLA approach with the same settings as we used to interpolate fecal pellet and DVM fluxes. The extent to which *Oithona* and *Oncaea* drew down surface-layer fecal pellet concentration ranged between 1-1000 ppm, i.e. 0.1 % at the most. Highest fractions were found in the southern central part of the study area where *Oncaea* regularly occurs[22], as well as in the European and Northern American shelf seas, where *Oithona* is common[22]. In the areas of highest observed fecal pellet fluxes, the effect of surface-layer copepod coprophagy was generally lower.

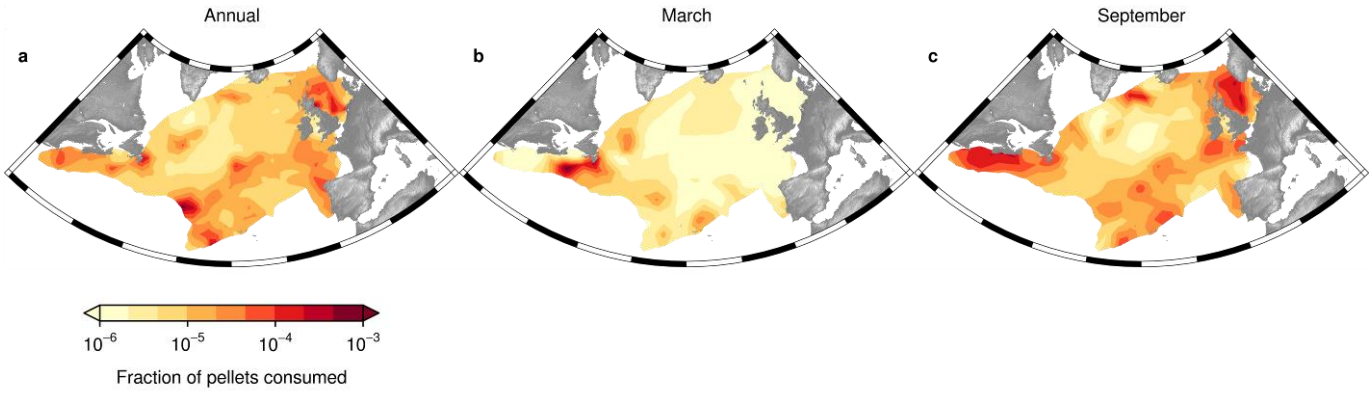

Supplementary Figure 9: Fraction of fecal pellet carbon concentration consumed by coprophageous surface-layer copepods in the period 2004-2014. Spatial distribution of annual mean is shown in panel (a); estimates for March in panel (b); and estimates for September in panel (c).

Relationship between recent NPP change and change in carbon fluxes

Spatially-resolved data on net primary productivity in the North Atlantic only exists since the launch of the Sea-Viewing Wide Field-of-View Sensor (SeaWiFS) program in late 1997. We were therefore not able to fully compare how the temporal trends in carbon fluxes

through copepods matched changes in net primary productivity. However, by combining VGPM-algorithm-based estimates of NPP[23] from SeaWiFS and Moderate Resolution Imaging Spectroradiometer (MODIS) satellites (www.science.oregonstate.edu/ocean.productivity/), we could obtain at least a rough estimate of NPP change between the two most recent periods of carbon flux estimates.

For the periods 1997-2003 and 2004-2014 we estimated mean annual NPP and investigated how their difference relates to change in modeled carbon fluxes. For both periods we calculated annual means from the monthly estimates of March to November (remaining months were considered zero, as for fecal pellet and DVM flux estimates) and aggregated the data to 1°×1° horizontal resolution. Since no consistent NPP data set exists for the entire period, we estimated the first period from SeaWiFS-based NPP estimates and the second period from MODIS-based NPP estimates. We compared the consistency between the two data sets for the overlapping years 2004-2008. The distributions of annual means from these periods were very similar (Pearson correlation coefficient was 0.97) but MODIS-based NPP estimates were on average 5.6 mg C m^{-2} y^{-1} lower, for which we corrected before we calculated the difference between the two periods (Supplementary Figure 10a). In addition, we ran Spearman correlation tests between NPP changes and changes of mixed layer fecal pellet fluxes, mixed layer DVM fluxes and hibernation fluxes at 500 meters at the 1°×1° resolution. Note that this comparison is somewhat compromised by the mismatch in the first periods considered (1997-2003 for NPP and 1993-2003 for modeled carbon fluxes).

While NPP as well as modeled carbon fluxes mainly increased at higher latitudes during the last two decades, changes in space were only weakly related. NPP increased for the majority of pixels above about 53° North (Supplementary Figure 10a,b) while, carbon fluxes increased mainly above 60° North (Supplementary Figure 10c-e). The correlation

between changes in NPP and changes in fecal pellet flux was weakly positive (Spearman correlation $r = 0.08$, $p \leq 0.01$), the correlation with changes in DVM flux was non-significant ($r = -0.06$, $p > 0.01$), and the one with changes in hibernation flux was even slightly negative ($r = -0.11$, $p \leq 0.01$).

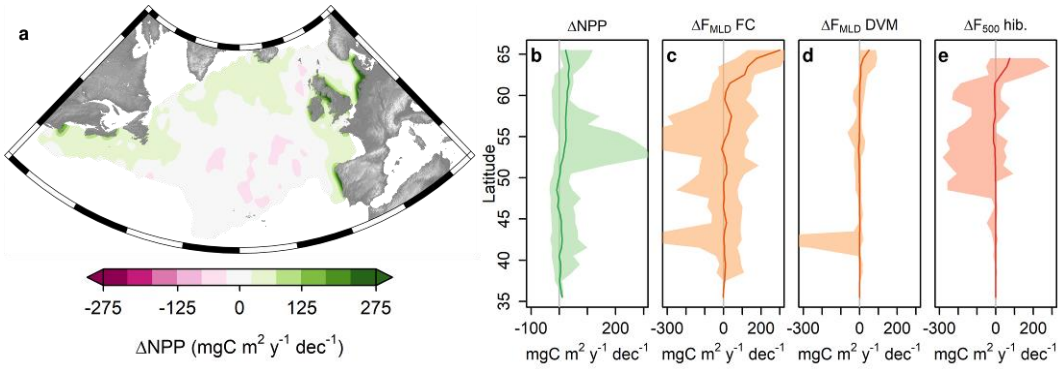

Supplementary Figure 10: Figure S2: NPP change between 1997-2003 and 2004-2014 and comparison to corresponding changes in modeled carbon fluxes. Spatial distribution of decadal changes in NPP (a) as well as medians (lines) and 90%-confidence intervals (polygons) of changes of NPP (b), mixed layer fecal pellet flux (c), mixed layer DVM flux (d) and hibernation flux at 500 meters (e) against latitude. Flux changes are shown between the periods 1993-2003 and 2004-2014.

Supplementary Discussion

Here, we built a comprehensive framework that describes numerous processes contributing to carbon fluxes mediated by surface-layer copepods. To be able to make quantitative estimates, we had to simplify these processes and make limiting assumptions. Furthermore, the observational data we used, although being perhaps the best of its kind, is not a perfect reflection of the situation in the surface waters of the North Atlantic. Below we discuss some major sources of uncertainty in our analysis related to data, feeding, and carbon transport.

Our data underestimated the abundance of small copepods and ignored the intraspecific variability of traits. The 270 µm mesh of the Continuous Plankton Recorder sampling device retains copepods with prosome lengths below one millimeter with reduced efficiency[24]. While attempts have been made to correct for this[25], finding a general way to do so is difficult, because in areas of high abundance the mesh can clog and retain locally higher fractions of small copepods. However, this limitation may have a restricted effect on flux estimates as small individuals contribute proportionally less to carbon fluxes than the well-sampled large ones. Besides not covering the entire community, the observations contain variability induced by high population dynamics and water dispersal processes which could make it difficult to robustly identify the duration of the feeding season of hibernating *Calanus* species. Also our the trait data used had limitations: we had to rely on crude, taxon-wise averages and empirical relationships, ignoring the sometimes significant intraspecific variation[4]. In the future, observational data from *in-situ* imaging surveys[26] may resolve some of these issues.

948 We had to make crude assumptions about the amount of the food consumed and the
949 duration of the feeding period. By relying on size-resolved phytoplankton biomass
950 estimates[27], we employed a novel way to accurately estimate the amount of food available to
951 copepods from remotely-sensed information. Still, we had no direct information on the
952 amount of heterotrophic food, such as within sinking and suspended particles, as well as on
953 food quality. Food quality influences feeding rates, digestion time, assimilation efficiency as
954 well as structure and sinking properties of fecal pellets[28]. We further assumed that the feeding
955 period was restricted to the time spent in the surface layer. Previous work in the field
956 generally supports this assumption[29,30], but these measurements are based on chlorophyll *a*
957 fluorescence and may underestimate the contribution of heterotrophic prey.

958 Finally, there are uncertainties related to carbon transport in all modeled fluxes. Fecal
959 pellets can undergo significant repackaging and fragmentation by zooplankton communities
960 in deeper water layers[28]. This leads to the production of both small fragments and new,
961 compact pellets impacting transport efficiency in ways that are poorly understood. Similarly,
962 mortality during hibernation is an important but poorly understood process. We assumed it to
963 be relatively low (0.001 d^{-1}) but small changes in this parameter can significantly impact
964 carbon flux estimates[31]. In the case of daily vertical migration, migration depth is challenging
965 to estimate, as both feeding loss and gain through lower mortality are weakly constrained.
966 Since we assumed no feeding during migration, our feeding loss estimates may be rather
967 high. In order to obtain realistic migration depths[32] we also assumed a high gain from reduced
968 mortality (mortality factor[9] = 50).

969

References

1. Holm, M. W. *et al.* Resting eggs in free living marine and estuarine copepods. *J. Plankton Res.* 1–14 (2017). doi:10.1093/plankt/fbx062

2. Hays, G. C., Proctor, C. A., John, A. W. G. & Warner, A. J. Interspecific differences in the diel vertical migration of marine copepods: The implications of size, color, and morphology. *Limnol. Oceanogr.* **39,** 1621–1629 (1994).

3. Hays, G. C. Large-scale patterns of diel vertical migration in the North Atlantic. *Deep Sea Res. Part I Oceanogr. Res. Pap.* **43,** 1601–1615 (1996).

4. Brun, P., Payne, M. R. & Kiørboe, T. A trait database for marine copepods. *Earth Syst. Sci. Data* **9,** 99–113 (2017).

5. Razouls, C., de Bovée, F., Kouwenberg, J. & Desreumaux, N. Diversity and Geographic Distribution of Marine Planktonic Copepods. Available at: http://copepodes.obs-banyuls.fr/en. (Accessed: 25th January 2016)

6. Halvorsen, E. Significance of lipid storage levels for reproductive output in the Arctic copepod Calanus hyperboreus. *Mar. Ecol. Prog. Ser.* **540,** 259–265 (2015).

7. Böttger-Schnack, R. & Schnack, D. Population structure and fecundity of the microcopepod Oncaea bispinosa in the Red Sea; a challenge to general concepts for the scaling of fecundity. *Mar. Ecol. Prog. Ser.* **302,** 159–175 (2005).

8. Richardson, A. J. *et al.* Using continuous plankton recorder data. *Prog. Oceanogr.* **68,** 27–74 (2006).

9. Hansen, A. N. & Visser, A. W. Carbon export by vertically migrating zooplankton: an optimal behavior model. *Limnol. Oceanogr.* **61,** 701–710 (2016).

10. Kiørboe, T. & Hirst, A. G. Shifts in Mass Scaling of Respiration, Feeding, and Growth Rates across Life-Form Transitions in Marine Pelagic Organisms. *Am. Nat.* **183,** E118–E130 (2014).

11. Brun, P., Payne, M. R. & Kiørboe, T. Trait biogeography of marine copepods - an analysis across scales. *Ecol. Lett.* **19,** 1403–1413 (2016).

12. Brent, R. P. *Algorithms for Minimization without Derivatives*. (Prentice-Hall, 1973).

13. Nelder, J. A. & Mead, R. A Simplex Method for Function Minimization. *Comput. J.* **7,** 308–313 (1965).

14. Iversen, M. H. & Ploug, H. Temperature effects on carbon-specific respiration rate and sinking velocity of diatom aggregates – potential implications for deep ocean export processes. *Biogeosciences* **10,** 4073–4085 (2013).

15. Marsay, C. M. *et al.* Attenuation of sinking particulate organic carbon flux through the mesopelagic ocean. *Proc. Natl. Acad. Sci.* **112,** 1089–1094 (2015).

16. McDonnell, A. M. P., Boyd, P. W. & Buesseler, K. O. Effects of sinking velocities and microbial respiration rates on the attenuation of particulate carbon fluxes through the mesopelagic zone. *Global Biogeochem. Cycles* **29,** 175–193 (2015).

17. Martin, J. H., Knauer, G. A., Karl, D. M. & Broenkow, W. W. VERTEX: carbon cycling in the northeast Pacific. *Deep Sea Res. Part A. Oceanogr. Res. Pap.* **34,** 267–285 (1987).

18. Boyd, P. W. & Trull, T. W. Understanding the export of biogenic particles in oceanic waters: Is there consensus? *Prog. Oceanogr.* **72,** 276–312 (2007).

19. Turner, J. T. Zooplankton fecal pellets, marine snow, phytodetritus and the ocean's biological pump. *Prog. Oceanogr.* **130,** 205–248 (2015).

20. Svensen, C. Is sedimentation of copepod faecal pellets determined by cyclopoids? Evidence from enclosed ecosystems. *J. Plankton Res.* **25,** 917–926 (2003).

21. Møller, E. F. *et al.* Production and fate of copepod fecal pellets across the Southern Indian Ocean. *Mar. Biol.* **158,** 677–688 (2011).

22. Barnard, R. *et al.* Continuous plankton records: Plankton Atlas of the north Atlantic Ocean (1958-1999). II. Biogeographical charts. *Marine Ecology Progress Series* 11–75 (2004).

23. Behrenfeld, M. J. & Falkowski, P. G. Photosynthetic rates derived from satellite-based chlorophyll concentration. *Limnol. Oceanogr.* **42,** 1–20 (1997).

24. Hays, G. C. Mesh selection and filtration efficiency of the Continuous Plankton Recorder. *J. Plankton Res.* **16,** 403–412 (1994).

25. PITOIS, S. & FOX, C. Long-term changes in zooplankton biomass concentration and mean size over the Northwest European shelf inferred from Continuous Plankton Recorder data. *ICES J. Mar. Sci.* **63,** 785–798 (2006).

26. Karsenti, E. *et al.* A Holistic Approach to Marine Eco-Systems Biology. *PLoS Biol.* **9,** e1001177 (2011).

27. Kostadinov, T. S., Milutinović, S., Marinov, I. & Cabré, A. Carbon-based phytoplankton size classes retrieved via ocean color estimates of the particle size distribution. *Ocean Sci.* **12,** 561–575 (2016).

28. Steinberg, D. K. & Landry, M. R. Zooplankton and the Ocean Carbon Cycle. *Ann. Rev. Mar. Sci.* **9,** 413–444 (2017).

29. Dagg, M. J., Frost, B. W. & Newton, J. Diel vertical migration and feeding in adult female Calanus pacificus, Metridia lucens and Pseudocalanus newmani during a spring bloom in Dabob Bay, a fjord in Washington USA. *J. Mar. Syst.* **15,** 503–509 (1998).

30. Atkinson, A., Ward, P. & Murphy, E. J. Diel periodicity of Subantarctic copepods: relationships between vertical migration, gut fullness and gut evacuation rate. *J. Plankton Res.* **18,** 1387–1405 (1996).

31. Visser, A. W., Grønning, J. & Jónasdóttir, S. H. Calanus hyperboreus and the lipid pump. *Limnol. Oceanogr.* **62,** 1155–1165 (2017).

32. Ohman, M. D. & Romagnan, J.-B. Nonlinear effects of body size and optical attenuation on Diel Vertical Migration by zooplankton. *Limnol. Oceanogr.* **61,** 765–770 (2016).

1051

1052

1053